Site dilution in the half-filled one-band Hubbard model: Ring exchange, charge fluctuations, and application to $La_2Cu_{1-x}(Mg/Zn)_xO_4$

J.-Y. P. Delannoy,[1,2] A. G. Del Maestro,[3] M. J. P. Gingras,[2,4,5] and P. C. W. Holdsworth[1]
[1]*Laboratoire de Physique, École Normale Supérieure de Lyon, 46 Allée d'Italie, 69364 Lyon Cedex 07, France*
[2]*Department of Physics and Astronomy, University of Waterloo, Ontario, Canada N2L 3G1*
[3]*Department of Physics, Harvard University, Cambridge, Massachusetts 02138, USA*
[4]*Canadian Institute for Advanced Research, 180 Dundas Street West, Toronto, Ontario, Canada M5G 1Z8*
[5]*Department of Physics and Astronomy, University of Canterbury, Private Bag 4800, Christchurch, New Zealand*
(Received 30 June 2008; published 12 June 2009)

We study the ground-state quantum spin fluctuations around the Néel ordered state for the one-band (t,U) Hubbard model on a site-diluted square lattice. An effective spin Hamiltonian $H_s^{(4)}$ is generated using the canonical transformation method, expanding to order $t(t/U)^3$. $H_s^{(4)}$ contains four-spin ring exchange terms as well as second- and third-neighbor bilinear spin-spin interactions. Transverse spin fluctuations are calculated to order $1/S$ using a numerical real-space algorithm first introduced by Walker and Walstedt [Phys. Rev. B **22**, 3816 (1980)]. Additional quantum charge fluctuations appear to this order in t/U, coming from electronic hopping and virtual excitations to doubly occupied sites. The ground-state staggered magnetization on the percolating cluster decreases with site dilution x, vanishing very close to the percolation threshold. We compare our results in the Heisenberg limit, $t/U \to 0$, with quantum Monte Carlo (QMC) results on the same model and confirm the existence of a systematic x-dependent difference between $1/S$ and QMC results away from $x=0$. For finite t/U, we show that the effects of both the ring exchange and charge fluctuations die away rapidly with increasing t/U. We use our finite t/U results to make a comparison with results from experiments on $La_2Cu_{1-x}(Mg/Zn)_xO_4$.

DOI: 10.1103/PhysRevB.79.224414 PACS number(s): 71.27.+a, 71.10.−w, 75.10.Jm

I. INTRODUCTION

A. Random disordered magnets

Magnetic materials and model magnetic systems are perhaps the best test benches for the study of collective phenomena in nature. This is particularly true in the context of systems with frozen or quenched random disorder.[1,2] Here, questions such as the sharpness of phase transitions in disordered systems,[3] the stability of ground-state symmetry-breaking (random-field) perturbations,[4] and spin-glass behavior arising from random frustration[5] have come under sharp scrutiny over the past 30 years.

The 1987 discovery of high-temperature superconductivity in doped antiferromagnetic copper oxide materials generated a huge amount of interest in quantum antiferromagnets which continues to this day.[6,7] Here, the magnetic properties depend strongly on the different possible types of quenched disorder and this has proven to be a rich source of novel quantum phenomena. An important area of investigation has been to explore how the ground state of insulating quantum magnets evolves as the level of random disorder is changed. The following examples represent a small subset of this class of studies. A large effort has been targeted toward understanding the properties of antiferromagnetic spins chains subject to various types of disorder.[8–10] Further work investigated how long-range order develops in two- and three-dimensional arrays of weakly coupled integer (Haldane) spin chains[8] and even-leg ladders.[11] The question of how Néel order develops upon magnetically diluting pure systems with quantum spin liquid ground states is another field of intensive study.[12]

Theoretical problems relating to various types of random bond disorder, as opposed to the more material-relevant case of site dilution, have also been investigated.[13,14] In three-dimensional systems, one noteworthy example is the so-called antiglass phenomenon in $LiHo_xY_{1-x}F_4$, where for a low concentration x of magnetic Ho^{3+} ions, the dipolar spin-glass phase seemingly disappears.[15] Another interesting problem concerns the role frozen random impurities may play at conventional and deconfined quantum critical points in two-dimensional antiferromagnets.[16] However, among the multitude of interesting problems, a particular one, possibly because of its seemingly simple physical setting and its broad conceptual appeal, has drawn considerable attention: that of the evolution of the antiferromagnetic Néel ground state in the site-diluted $S=1/2$ nearest-neighbor (NN) square lattice Heisenberg antiferromagnet (SLHAF).

B. Site-diluted SLHAF and $La_2Cu_{1-x}(Mg/Zn)_xO_4$

As the insulating and antiferromagnetic parent of high-temperature superconductivity in $La_{2-x}Sr_xCuO_4$, La_2CuO_4 has quasi-two-dimensional magnetic exchange interactions, a good starting point for its description is to treat the CuO_2 planes as decoupled SLHAFs. Hence, early experimental studies on zinc and magnesium substitution for copper in La_2CuO_4 (Refs. 17 and 18) provided some of the earliest motivation and interest in the problem of site-diluted SLHAFs.[19] In particular, Cheong *et al.*[18] found from bulk thermodynamic measurements that in the diluted $S=1/2$ quantum antiferromagnetic materials, $La_2Cu_{1-x}Zn_xO_4$ and $La_2Cu_{1-x}Mg_xO_4$, the Néel temperature T_N vanishes faster than in other materials that can be considered as site-diluted classical square lattice magnetic systems (either because they

 ©2009 The American Physical Society

have large spin S, or because they have large Ising anisotropies).

Most importantly, these early experimental results suggested that T_N, hence long-range antiferromagnetic Néel order, may vanish at a critical impurity concentration x_c less than the site-dilution percolation threshold for the square lattice, $x_p \approx 0.41$. This possibility was seemingly supported by subsequent muon-spin-relaxation (μSR) and nuclear-quadrupole-resonance (NQR) experiments,[20] with these latter measurements also suggesting the possibility of a second transition below $T_N(x)$ into a spin-glass-like state.

From a classical point of view, the ground state of the SLHAF has two-sublattice Néel order for all $x < x_p$. Consequently, early experiments[18,20] on site-diluted La_2CuO_4 implied that either a novel quantum ground state develops in the site-diluted SLHAF for $x_c < x < x_p$, or that *frustrating* farther-neighbor exchange interactions are important in the real material and that these drive the system into a two-dimensional Heisenberg spin-glass ground state, presumably via the proliferation of Villain canted states for $x_c < x < x_p$.[21–26]

The idea that Néel order could disappear in the diluted SLHAF, due to quantum effects, for a concentration of magnetic moments less than the geometric site percolation threshold x_p had been suggested by some,[27] but not all,[19,28] early calculations. In strong contrast to the early body of experimental evidence[18,20] and a theoretical suggestion,[27] numerical[19] and theoretical[28] calculations as well as large scale quantum Monte Carlo (QMC) simulations[29,30] on the diluted SLHAF find that Néel order survives up to the percolation threshold x_p. Further, contrary to earlier experiments,[18,20] recent neutron-scattering studies on single crystals of $La_2Cu_{1-x}(Mg/Zn)_xO_4$ found that long-range Néel order does survive up to at least $x=0.39$, if not up to x_p.[31,32] Interestingly, recent QMC studies show that the same scenario holds for homogeneous bond dilution, with exotic quantum phases appearing only for inhomogeneous dilution where local ladder structures form.[14]

A proposed explanation for the discrepancy between the earlier experiments[17,18,20] and the more recent ones[31,32] is that samples are extremely sensitive to excess oxygen, or off-stoichiometric δ, $La_2CuO_{4+\delta}$, as Cu^{2+} is substituted by either Zn^{2+} or Mg^{2+}. Off-stoichiometry with $\delta > 0$ is hole doping, which is extremely detrimental to long-range Néel order. Thus, the present picture, supported by both numerical[19,29,30] and experimental[31,32] studies, is that Néel order survives in the site-diluted SLHAF (Refs. 29 and 30) and in $La_2Cu_{1-x}(Mg/Zn)_xO_4$ (Refs. 31 and 32) up to x_p, with no intervening exotic quantum ground state for $x < x_p$.

C. Quantum Monte Carlo versus $La_2Cu_{1-x}(Mg/Zn)_xO_4$

While both high-precision QMC studies of the site-diluted SLHAF (Ref. 30) and neutron-scattering experiments[31,32] on $La_2Cu_{1-x}(Mg/Zn)_xO_4$ now find that the Néel order survives up to $x_c \approx x_p$ (exactly $x_c = x_p$ for the QMC simulations), the quantitative agreement stops here. There is a systematic discrepancy between QMC and the neutron results for the sublattice Néel order parameter $[M(x)]$ as a function of x. The experimental and numerical data are reproduced in Fig. 1. In this figure, the QMC results of Ref. 30 are shown by the upper solid line. The experimental results (squares: neutron, from Ref. 31; triangles: NQR, from Ref. 20) lie on the dashed line, which is a guide for the eyes parametrized by $[M(x)]/M(0) = (1 - x/x_p)^{\beta_{\text{eff}}}$. The QMC results lie above the experimental data over the whole range $0 < x < x_p$, as illustrated by the shaded region. Taking it as a premise that the QMC data are essentially the exact results for the diluted $S = 1/2$ SLHAF, the systematic difference between them and the experimental data shown in Fig. 1 suggests that Zn^{2+}- and Mg^{2+}-substituted Cu^{2+} in La_2CuO_4 are not quantitatively described by a site-diluted nearest-neighbor Heisenberg Hamiltonian. The nature of the discrepancy is in itself interesting. It is initially small at low x, increases and reaches a maximum for $x \sim 0.35$, and decreases upon approaching x_p such that the "true" underlying microscopic Hamiltonian describing $La_2Cu_{1-x}(Mg/Zn)_xO_4$ seems to also possess a percolation threshold very close to that of the idealized SLHAF.

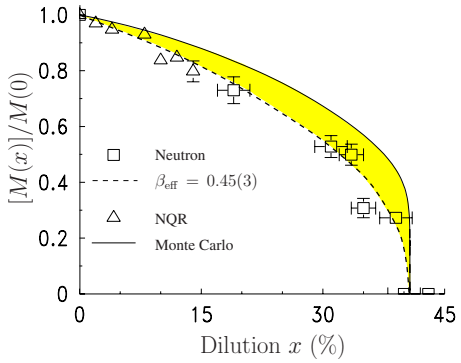

FIG. 1. (Color online) Ground-state staggered magnetization $[M(x)]$ as a function of concentration x of Zn and Mg in $La_2Cu_{1-x}(Mg/Zn)_xO_4$, normalized to the value for zero dilution, $M(0)$ (Ref. 31). The solid line shows the results from quantum Monte Carlo (Ref. 30) for the site-diluted SLHAF. The figure is reproduced from Ref. 31.

D. Ring exchange interactions

One class of candidate perturbations that may give the missing physics of diluted La_2CuO_4 is that of ring, or cyclic, exchange interactions involving multiple interactions around closed plaquettes of the square lattice. Such interactions have received intensive attention recently[33–35] and have been shown to play an important role in the quantitative description of undiluted La_2CuO_4.[36–39] Taking as a starting point the one-band half-filled Hubbard model,[40–42] the lowest-order ring exchange interaction takes its origin in virtual electronic hopping processes, fourth order in t/U, taking electrons coherently around a closed square plaquette. Here t is the nearest-neighbor hopping constant and U is the on-site Coulomb energy. Taking it as plausible[37–39] that ring exchange is indeed present and a leading perturbation beyond the Heisenberg model description of La_2CuO_4, it is natural to ask what its effect is on the Néel order parameter upon substituting Cu by a concentration x of nonmagnetic ions (see Fig. 1). This is the question we explore in this paper.

To tackle this question, one must return to a problem of correlated electrons. The reason is that the spin-only Hamiltonian with ring exchange derives from a set of electronic hops. As we show below, the elimination of an intermediate site in an electron hopping pathway affects the resulting effective spin Hamiltonian in a nontrivial manner. Specifically, we consider the problem of a site-diluted half-filled one-band Hubbard model away from the Heisenberg $t/U \to 0$ limit. Since here ring exchange originates solely from correlated nearest-neighbor electronic hops, they cannot move the percolation threshold to a larger value than the nearest-neighbor threshold x_p. From this constraint alone, ring exchange is an admissible candidate for a perturbation to the diluted $S=1/2$ SLHAF, as it preserves the same geometric percolation threshold x_p as the nearest-neighbor Heisenberg model.

The presence of the ring exchange and second- and third-nearest-neighbor bilinear exchange terms in the Hamiltonian, generated by hopping processes to fourth order in t/U, leads to a sign problem for currently available QMC methods using the standard S^z basis representation of the Hamiltonian.[43] A direct attack on the site-diluted ring exchange Hamiltonian via QMC, such as done for the site-diluted Heisenberg model,[30] is therefore not possible at this time. As a first step in investigating the role played by ring exchange in the site-diluted Hubbard model, we carry out a finite-lattice spin-wave calculation to order $1/S$ on an extended effective spin Hamiltonian generated from up to four hop electronic pathways. To proceed, we use a real-space linear spin-wave method adapted to finite-size diluted lattices, first developed by Walker and Walstedt[44] in the context of spin glasses and similar to that used for the site-diluted nearest-neighbor Heisenberg antiferromagnet on the square[45] and honeycomb lattices.[46] We investigate the role of ring exchange on the dependence of the ground-state staggered magnetization $[M(x)]$ as a function of x. In Ref. 45, it was found that there is a systematic difference between the value of this quantity, calculated via the spin-wave method, and the essentially exact QMC.[30] From this, it is clear that a similar systematic difference should also exist between our data calculated using a $1/S$ expansion and what would be the exact value for $[M(x)]$, as a function of dilution for the extended Hamiltonian. Hence, although the main motivation for this project comes from the experiment on $La_2Cu_{1-x}(Mg/Zn)_xO_4$,[31] some care has to be taken in attempting to make a direct comparison with experimental results. Rather, our results for the extended Hamiltonian and electronic hopping can be quantitatively benchmarked by a comparison with those for the site-diluted Heisenberg model, using the same real-space expansion technique. From a broader perspective, our work provides a glimpse at the role of charge-correlation effects in the problem of diamagnetic site dilution in the one-band Hubbard model.

E. Charge fluctuations

The generation of ring and farther-neighbor exchange interactions is not the only effect of extending the analysis of the one-band Hubbard model beyond the Heisenberg limit using a perturbation expansion in t/U. We have previously shown that extending the expansion to order $(t/U)^4$ generates quantum charge fluctuations[42] that are independent of the transverse spin fluctuations of localized $S=1/2$ moments. These fluctuations appear in the perturbation expansion on the square lattice because, to this order, the ground-state wave function contains an admixing with excited states corresponding to doubly occupied sites. As doubly occupied sites carry no moment, the expectation value for the magnetic moment of the Hubbard model is reduced below that expected from the effective spin-only Hamiltonian describing transverse spin fluctuations. We show here that these charge fluctuations are a key element in the ultimate success of comparisons between the one-band Hubbard model and experiments on both undiluted and site-diluted La_2CuO_4. Just as for ring exchange effects, we find that the effects of charge fluctuations disappear as the site percolation threshold is approached, as four hop electronic processes are interrupted by the dilution well before this limit is reached.

The rest of the paper is organized as follows: before launching into the calculations, we discuss in Secs. II A and II B some of the caveats that arise when considering a low-energy effective spin-only Hamiltonian derived from a site-diluted Hubbard model. In particular, the exchange interactions become explicitly disorder dependent (Sec. II A). Furthermore, by going beyond the Heisenberg limit, the operator for the Néel order parameter has to be corrected to take into account the charge mobility of the electrons in the Hubbard model.[42] The results presented below show that this correction is crucially important to obtain the correct $1/S$ behavior of the model. The consequent reduction in the amplitude of the staggered magnetization in the presence of local disorder is discussed in Sec. II B. We then discuss in Sec. II C the stability of the classical Néel ground state for finite disorder, when ring exchange is present. Section II D describes the spin-wave method that we use. Section III gives an overview of the algorithmic procedure used to diagonalize the quadratic form of the disordered finite-lattice spin Hamiltonian. The numerical results are presented in Section IV, followed in Sec. V by a discussion of the results and a perspective for future work. Appendixes A and B discuss the question of statistical uncertainties in the data presented in Sec. IV.

II. SPIN HAMILTONIAN AND REAL-SPACE LINEAR SPIN-WAVE CALCULATION

A. Spin Hamiltonian

We begin with the Hubbard Hamiltonian H_H:

$$H_H = T + V \tag{2.1}$$

$$= -t \sum_{i,j;\sigma}{}' \epsilon_i \epsilon_j c^\dagger_{i,\sigma} c_{j,\sigma} + U \sum_i{}' \epsilon_i n_{i,\uparrow} n_{i,\downarrow}. \tag{2.2}$$

The first term is the kinetic-energy term that destroys an electron of spin σ at site j and creates one on the nearest-neighbor site i. The second term is the on-site Coulomb energy U for two electrons with opposite spins to be on the same site i and where $n_{i,\sigma}=c^\dagger_{i,\sigma}c_{i,\sigma}$ is the occupation operator

at site i. A site i substituted by a nonmagnetic cation has $\epsilon_i=0$; otherwise $\epsilon_i=1$. In the following we use the notation Σ' to represent a summation over the L^2 sites of the square lattice and Σ for a sum over the $N=\Sigma_i'(1-\epsilon_i)$ undiluted sites. The number of magnetic sites (and hence of mobile electrons, N) at half filling is thus configuration dependent. The average concentration of vacancies is $1-[\epsilon_i]_{\text{disorder}}=x$. Similarly, Σ_j' represents a sum over neighboring sites and Σ_j represents a sum over neighboring occupied magnetic sites. Below, a summation index with angular brackets $\langle\cdots\rangle$ in $\Sigma_{\langle\cdots\rangle}$ denotes an ordered sum, taking into account only unique pathways.

The derivation of a spin Hamiltonian from a one-band Hubbard model can be performed through many different methods, leading to apparently different effective spin Hamiltonians. It is only recently that it has been shown[41] that all these Hamiltonians are equivalent, as they are related to each other through a unitary transformation. We have recently applied the canonical transformation method, which uses the ratio t/U as a small parameter in a perturbation expansion, to study the magnetic excitations and the staggered magnetization in the Hubbard model.[42,47] The method, introduced by Harris and Lange[48] and developed further by MacDonald *et al.*,[40,49,50] relies on the separation of the kinetic part T of the Hubbard Hamiltonian into three terms that respectively increase by 1 (T_1), keep constant (T_0), or decrease by 1 (T_{-1}) the number of doubly occupied sites. Specifically, one writes

$$T=-t\sum_{i,j;\sigma}{}' \epsilon_i\epsilon_j c_{i,\sigma}^{\dagger}c_{j,\sigma}=T_1+T_0+T_{-1}, \tag{2.3}$$

$$T_1=-t\sum_{i,j;\epsilon_i\epsilon_j\sigma}{}' \epsilon_i\epsilon_j n_{i,\bar{\sigma}}c_{i,\sigma}^{\dagger}c_{j,\sigma}h_{j,\bar{\sigma}}, \tag{2.4}$$

$$T_0=-t\sum_{i,j;\sigma}{}' \epsilon_i\epsilon_j (h_{i,\bar{\sigma}}c_{i,\sigma}^{\dagger}c_{j,\sigma}h_{j,\bar{\sigma}}+n_{i,\bar{\sigma}}c_{i,\sigma}^{\dagger}c_{j,\sigma}n_{j,\bar{\sigma}}), \tag{2.5}$$

$$T_{-1}=-t\sum_{i,j;\sigma}{}' \epsilon_i\epsilon_j h_{i,\bar{\sigma}}c_{i,\sigma}^{\dagger}c_{j,\sigma}n_{j,\bar{\sigma}}, \tag{2.6}$$

where $\bar{\sigma}$ stands for up if σ is down and for down if σ is up and where $h_{i,\bar{\sigma}}=1-n_{i,\bar{\sigma}}$. This separation comes from multiplying the kinetic term T on the right by $n_{i,\bar{\sigma}}+h_{i,\bar{\sigma}}=1$ and multiplying on the left by $n_{j,\bar{\sigma}}+h_{j,\bar{\sigma}}=1$.

Applying a unitary transformation e^{iS} to H_H leads to a spin-only Hamiltonian, H_s, through the relation

$$H_s=e^{iS}H_He^{-iS}=H_H+\frac{[iS,H_H]}{1!}+\frac{[iS,[iS,H_H]]}{2!}+\cdots. \tag{2.7}$$

We do not reproduce the derivation here; rather we refer the reader to Refs. 40, 42, and 47 for details of the form of S and H_H order by order in the development. Up to third order in the t/U expansion, we finally find for the effective spin Hamiltonian

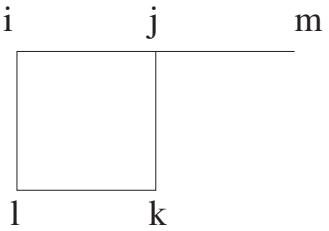

FIG. 2. Labels for the different sites involved in the effective spin interactions and arising from a t-U Hubbard model up to order $t(t/U)^3$. $\langle i,j\rangle$, $\langle\langle i,k\rangle\rangle$, and $\langle\langle\langle i,m\rangle\rangle\rangle$ are nearest-, second-nearest, and third-nearest neighbors, respectively. $\langle i,j,k,l\rangle$ denotes the sites that belong to an elementary square plaquette.

$$H_s^{(4)}=\sum_{\langle i,j\rangle}J_1(\boldsymbol{S}_i\cdot\boldsymbol{S}_j)+\sum_{\langle\langle i,k\rangle\rangle}J_2(\boldsymbol{S}_i\cdot\boldsymbol{S}_k)+\sum_{\langle\langle\langle i,m\rangle\rangle\rangle}J_3(\boldsymbol{S}_i\cdot\boldsymbol{S}_m)+\sum_{\langle i,j,k,l\rangle}J_c\{(\boldsymbol{S}_i\cdot\boldsymbol{S}_j)(\boldsymbol{S}_k\cdot\boldsymbol{S}_l)+(\boldsymbol{S}_i\cdot\boldsymbol{S}_l)(\boldsymbol{S}_k\cdot\boldsymbol{S}_j)-(\boldsymbol{S}_i\cdot\boldsymbol{S}_k)(\boldsymbol{S}_j\cdot\boldsymbol{S}_l)\}, \tag{2.8}$$

where the site labels refer to the configuration shown in Fig. 2. The different coupling constants (J_1,J_2,J_3,J_c) arise as a result of the integration over all electronic paths allowed in the site-diluted Hubbard model. As a result, they depend on the local site occupancy along the exchange path. We find

$$J_1=4\left[\frac{t^2}{U}\epsilon_i\epsilon_j-\frac{t^4}{U^3}(4\epsilon_i\epsilon_j+\mathcal{N}_{ij})\right], \tag{2.9}$$

$$J_2=4\left[\frac{t^4}{U^3}(\epsilon_i\epsilon_j\epsilon_k+\epsilon_i\epsilon_l\epsilon_k-\mathcal{N}_{ik})\right], \tag{2.10}$$

$$J_3=4\left[\frac{t^4}{U^3}\epsilon_i\epsilon_j\epsilon_m\right], \tag{2.11}$$

$$J_c=80\left[\frac{t^4}{U^3}\epsilon_i\epsilon_j\epsilon_k\epsilon_l\right], \tag{2.12}$$

where $\mathcal{N}_{\mu\nu}$ is a plaquette index for bond $\mu\nu$ and is equal to the number of plaquettes to which both sites μ and ν belong. When there is no dilution, $\mathcal{N}_{\mu\nu}=2$ for all nearest-neighbor $\langle i,j\rangle$ bonds and 1 for second-neighbor bonds $\langle\langle i,j\rangle\rangle$ across the diagonal of a plaquette. When one site is removed, two of the nearest-neighbor $\mathcal{N}_{\mu\nu}$ are set to zero and the two remaining ones are reduced from 2 to 1. $\mathcal{N}_{\mu\nu}$ for the next-nearest-neighbor bond across the diagonal of the plaquette is reduced from 1 to 0. For example, consider Fig. 2, where only the site j has been eliminated by dilution. The expressions for the coupling constants become

$$J_1(i,l)=4\frac{t^2}{U}-20\frac{t^4}{U^3},$$

$$J_2(i,k)=4\frac{t^4}{U^3},$$

$$J_3(i,m)=0, \quad J_c(i,j,k,l)=0, \tag{2.13}$$

which should be compared with $J_1=4t^2/U-24t^4/U^3$, $J_2=J_3=4t^4/U^3$, and $J_c=80t^4/U^3$ for the undiluted lattice. The most important point here is that since the antiferromagnetic and frustrating J_2 and J_3 exist solely via electronic hopping processes connecting nearest-neighbor sites, these interactions are progressively eliminated as intermediate sites are diluted. That is, if both sites j and l are missing then $J_2(i,k)=0$. Hence, one can see that site dilution strongly affects the coupling constants as farther-neighbor exchange depends on the existence of a nearest-neighbor pathway between the sites. This would not be the case if the original Hubbard model included direct second- or third-nearest-neighbor hopping parameters, t' and t'', respectively.[47] We will return to this issue in Sec. IV. However, in this paper we limit ourselves to nearest-neighbor hopping only.

B. Néel order parameter

Our objective is to calculate the ground-state Néel order parameter for the original Hubbard model as a function of site dilution, using a spin-only description. To do this, the staggered (spin-density-wave) magnetization operator

$$\hat{M}_H=\frac{1}{N}\sum_i (-1)^i(n_i^{\uparrow}-n_i^{\downarrow}), \tag{2.14}$$

defined for the Hubbard model, must be canonically transformed before it can be exploited in a spin-only description. Here, $\hat{M}_H$, $\hat{M}_s$, and $\hat{\tilde{M}}_s$ refer to operators, while M_H, M_s, and $\tilde{M}_s$ refer to their expectation values. That is, within the effective theory $\hat{M}_H$ becomes $\hat{M}_s=e^{iS}\hat{M}_H e^{-iS}$ and the expectation value in the ground state is defined as

$$M_s=\frac{{}_H\langle 0|\hat{M}_H|0\rangle_H}{{}_H\langle 0|0\rangle_H}=\frac{{}_s\langle 0|\hat{M}_s|0\rangle_s}{{}_s\langle 0|0\rangle_s}. \tag{2.15}$$

Here $|0\rangle_H$ and $|0\rangle_s=e^{iS}|0\rangle_H$ are the ground-state wave vectors in the original Hubbard and spin-only models. We have recently shown[42] that this is more than just an academic point. Rather, it has important consequences for the ground-state magnetization as one moves into the intermediate-coupling regime and, as we will show below, plays a significant quantitative role in the present site-diluted Hubbard model. As we apply the canonical transformation on $\hat{M}_H$,[42,47] we find $\hat{M}_s$ to be

$$\hat{M}_s=\hat{M}_H+\frac{1}{U}(\tilde{T}_1-\tilde{T}_{-1})+\frac{1}{2U^2}(\tilde{T}_{-1}T_1-T_{-1}\tilde{T}_1), \tag{2.16}$$

where

$$\frac{1}{N}\tilde{T}_1\equiv[T_1,\hat{M}_H], \tag{2.17}$$

$$\frac{1}{N}\tilde{T}_{-1}\equiv[T_{-1},\hat{M}_H], \tag{2.18}$$

$$\frac{1}{N}\tilde{T}_0\equiv[T_0,\hat{M}_H]. \tag{2.19}$$

After some algebra, we can write this expression in terms of $S=1/2$ spin operators[42] as

$$\hat{M}_s=\frac{1}{N}{\sum_i}' \epsilon_i S_i^z(-1)^i-\frac{2t^2}{NU^2}{\sum_{\langle i,j\rangle}}' \epsilon_i\epsilon_j\{S_i^z-S_j^z\}(-1)^i. \tag{2.20}$$

Recalling the standard definition for the staggered magnetization operator in a spin model,

$$\hat{\tilde{M}}_s=\frac{1}{N}{\sum_i}' \epsilon_i S_i^z(-1)^i, \tag{2.21}$$

we arrive at the principal result of Ref. 42 that

$$M_s=\frac{{}_s\langle 0|\hat{M}_s|0\rangle_s}{{}_s\langle 0|0\rangle_s},$$

$$\tilde{M}_s=\frac{{}_s\langle 0|\hat{\tilde{M}}_s|0\rangle_s}{{}_s\langle 0|0\rangle_s},$$

$$M_s\neq\tilde{M}_s. \tag{2.22}$$

The difference is due to the appearance of new quantum fluctuations arising from the charge delocalization over closed virtual loops of electronic hops, which is the origin of the second term in Eq. (2.20). These spin-independent fluctuations, which appear to order t^2/U^2 in the magnetization operator, are generated when the canonical transformation is applied on the Hamiltonian to order t^4/U^3 and are therefore not present in the $(t/U\to 0)$ Heisenberg limit. We recently investigated the effects of these terms in the undiluted case.[42,47] Here, the disorder is manifested through the dilution variables ϵ_i. In this paper, we are interested in how the spin-renormalization factor modifies the ground-state magnetization upon site dilution. However, before doing so, we first return to a discussion of the ground state of the spin-only Hamiltonian $H_s^{(4)}$. Henceforth, for the sake of compactness, we shall omit the subscript "s" in M_s and $\tilde{M}_s$, understanding that all results presented below were obtained from calculations performed on a spin-only description of the low-energy sector of the half-filled Hubbard model.

C. Classical ground state

1. J_1 interactions only

The real-space spin-wave method that we use to deal with dilution requires, as the starting point, the knowledge of the classical ground-state spin configuration. With nearest-neighbor interactions only, the classical ground-state configuration is, in the absence of dilution, the Néel staggered spin configuration. This long-range-ordered state results from the local minimization of the exchange interactions. Since we work with a concentration of defects, or dilution x,

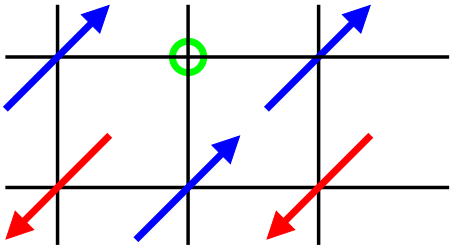

FIG. 3. (Color online) Diluted Néel configuration. The circle labels a missing (diluted) site.

smaller than the percolation threshold x_p, there exists a percolating cluster of magnetic sites with an exchange path connecting every pair of spins on the cluster. As a result, the classical ground-state configuration for the percolating cluster is a connected Néel configuration, where every spin keeps the orientation it would have had without dilution (see Fig. 3).

2. Full Hamiltonian

In the case of the effective spin-only Hamiltonian, expressed in Eq. (2.8), the situation becomes more complicated. If the J_2, J_3, or J_c interactions get too large, the system undergoes a phase transition to a different classical state that is not collinear.

3. Nondiluted case

As can be read from Eqs. (2.9)–(2.12), when there is no dilution, the coupling constants read

$$J_1 = 4\frac{t^2}{U} - 24\frac{t^4}{U^3},$$

$$J_2 = J_3 = 4\frac{t^4}{U^3},$$

$$J_c = 80\frac{t^4}{U^3}. \tag{2.23}$$

For $t/U=1/8$, a value similar to that reported for La_2CuO_4 and that we henceforth take in the present work,[36,47] the ratios between the different coupling constants are

$$\frac{J_2}{J_1} \simeq 0.0172,$$

$$\frac{J_3}{J_1} \simeq 0.0172,$$

$$\frac{J_c}{J_1} \simeq 0.0862. \tag{2.24}$$

For a model with nearest and next-nearest couplings only, the J_1/J_2 model, the Néel state is stable for $J_2/J_1 \leq 0.5$.[51–53] For the J_1/J_c model, the quantity $\tilde{J}_c = J_c S^2$ is usually introduced, and as long as $\tilde{J}_c \leq J/2$, the Néel state is stable.[54] Our parameters are far away from these critical values, and hence the classical ground state, without dilution, is Néel ordered.

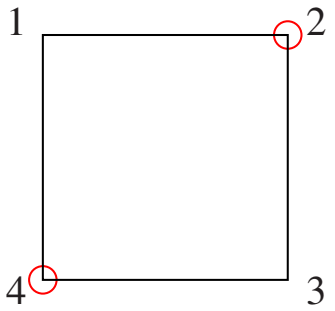

FIG. 4. (Color online) Particular dilution configuration. In this example, sites 2 and 4 are removed by dilution.

4. Diluted case

One might have expected that the combination of frustration, brought about by J_2 and J_3, and site dilution would trigger an instability in favor of a local Villain canting of the spins,[21] leading ultimately to a two-dimensional Heisenberg spin glass before x_p is reached.[26] However, as alluded to in the discussion below Eq. (2.13), such locally Villain canted states do not occur in the model considered here, where all effective magnetic interactions derive from electronic processes involving nearest-neighbor hopping. Specifically, as we saw in Sec. II A, for the configuration of diluted sites shown in Fig. 4, the second-neighbor interaction J_{13} between sites 1 and 3 is destroyed by the dilution of sites 2 and 4. As a consequence, as long as the critical ratios for the J_2/J_1, J_3/J_1, or J_c/J_1 for destroying two-sublattice collinear Néel order are not reached, there are no spins coupled by dominantly *random* frustrating interactions, J_2, J_3, or J_c, as can be verified from consideration of Eqs. (2.9)–(2.12).

We therefore conclude that the classical ground state of $H_s^{(4)}$ in Eq. (2.9) for $t/U=1/8$ on the percolation cluster is a Néel configuration for all concentrations below the percolation threshold. From this, one can immediately see the importance of the site percolation threshold in this problem: within the model considered, that is, the site-diluted one-band Hubbard model of Eq. (2.2), the only accessible classical ground state is Néel ordered all the way to the percolation threshold x_p. Hence, any reduction in the range of stability of the Néel ground state is due uniquely to quantum fluctuations and is not due to (classical) random frustration effects. This conclusion is explicitly verified *post factum* within the real-space spin-wave calculation presented below: any instability toward a noncollinear ground state would be detected as a negative eigenvalue of the Hessian matrix leading to complex eigenfrequencies. No such instabilities were detected in more than the 10 000 realizations of disorder considered in this work.

We note, however, that La_2CuO_4 is only approximately described by the one-band Hubbard model with nearest-neighbor hopping only. For instance, we have recently shown that one can achieve a quantitative improvement to the fitting of the spin-wave excitation spectrum measured by Coldea *et al.*[36] by including direct farther-neighbor hopping constants

t' and t''.[47] Such direct hops would likely change the above results, leading to canted classical ground states and a Heisenberg spin-glass phase[21–26] before the percolation threshold is reached ($x_c < x_p$).

D. Elementary excitations of a diluted spin-1/2 system

1. Method

The introduction of site dilution destroys translational invariance, which excludes the use of Fourier space for calculating the spin-wave excitations. Hence, we closely follow the method introduced by Walker and Walstedt[44] to study excitations in Heisenberg spin glasses. Other recent studies of site-diluted $S=1/2$ Heisenberg antiferromagnets have followed a similar approach.[45,46] We first summarize this method for the simplest case of nearest-neighbor exchange, J_1 only, with Hamiltonian

$$H = \frac{1}{2}\sum_{i\neq j} J_1(i,j)\boldsymbol{S}_i \cdot \boldsymbol{S}_j. \tag{2.25}$$

As we know the classical ground state of the system, we can define for each site i, a unit vector $\boldsymbol{n}_i^0$ pointing in the direction of the classical spin $\boldsymbol{S}_i$ in this state. Note that in Eqs. (2.14), (2.20), and (2.21) a unique global quantization axis in the laboratory frame, $\hat{z}$, was used to define $\tilde{M}_s$ and M_s. Henceforth, we label the spin components in terms of the projection of $\boldsymbol{S}_i$ along the axis of a local right-handed frame. We do so to keep with the original notation of Ref. 44, from which we borrowed the method we use here. Let $\{\boldsymbol{x}_i,\boldsymbol{y}_i,\boldsymbol{n}_i^0\}$ be an orthogonal triad of unit vectors and let $\boldsymbol{p}_i^+$ and $\boldsymbol{p}_i^-$ be vectors defined by

$$\boldsymbol{p}_i^+ = \frac{\boldsymbol{x}_i + i\boldsymbol{y}_i}{\sqrt{2}},$$

$$\boldsymbol{p}_i^- = \frac{\boldsymbol{x}_i - i\boldsymbol{y}_i}{\sqrt{2}}. \tag{2.26}$$

We also introduce spin deviation (boson creation and annihilation operators), a_i and $a_i^\dagger$, defined by

$$\boldsymbol{S}_i \cdot \boldsymbol{n}_i^0 = S - a_i^\dagger a_i, \tag{2.27}$$

$$\boldsymbol{S}_i \cdot \boldsymbol{p}_i^+ = \sqrt{2S}\left[1 - \frac{a_i^\dagger a_i}{2S}\right]^{1/2} a_i,$$

$$\boldsymbol{S}_i \cdot \boldsymbol{p}_i^- = \sqrt{2S}\, a_i^\dagger \left[1 - \frac{a_i^\dagger a_i}{2S}\right]^{1/2}, \tag{2.28}$$

where the spin components are defined with respect to the local basis set $\{\boldsymbol{x}_i,\boldsymbol{y}_i,\boldsymbol{n}_i^0\}$. With Eq. (2.27) and the definition of $\boldsymbol{p}_i^\pm$, we can rewrite Hamiltonian (2.25) to order $O(S)$ as

$$H = \frac{1}{2}S^2\sum_{i\neq j} J_{ij}\boldsymbol{n}_i^0 \cdot \boldsymbol{n}_j^0 + \frac{1}{2}S^{3/2}\sum_{i\neq j} J_{ij}[\boldsymbol{n}_i^0 \cdot \boldsymbol{p}_j^+ a_j^\dagger + \boldsymbol{n}_i^0 \cdot \boldsymbol{p}_j^- a_j + \boldsymbol{n}_j^0 \cdot \boldsymbol{p}_i^+ a_i^\dagger + \boldsymbol{n}_j^0 \cdot \boldsymbol{p}_i^- a_i] + \frac{1}{2}S\sum_{i\neq j} J_{ij}[(\boldsymbol{p}_i^+ a_i^\dagger + \boldsymbol{p}_i^- a_i)\cdot(\boldsymbol{p}_j^+ a_j^\dagger + \boldsymbol{p}_j^- a_j) - \boldsymbol{n}_i^0 \cdot \boldsymbol{n}_j^0 (a_i^\dagger a_i + a_j^\dagger a_j)]. \tag{2.29}$$

By making reference to the classical ground state, we introduce λ_i defined by

$$\lambda_i \boldsymbol{n}_i^0 \equiv \sum_j J_{ij}\boldsymbol{n}_j^0. \tag{2.30}$$

Physically, λ_i corresponds to the local staggered mean field at site i originating from all the spins $\boldsymbol{S}_j$ to which $\boldsymbol{S}_i$ is coupled. This change of variables makes clear that the second term of the Hamiltonian in Eq. (2.29) vanishes. We keep only the leading quantum correction to the classical term $\frac{1}{2}S^2\Sigma_{\langle i,j\rangle}J_{ij}\boldsymbol{n}_i^0\cdot\boldsymbol{n}_j^0$, H_2, quadratic in the $a_i^\dagger$ and a_i operators:

$$H_2 = -S\left[\sum_i \lambda_i a_i^\dagger a_i - \frac{1}{2}\sum_{i\neq j} J_{ij}(\boldsymbol{p}_i^+ a_i^\dagger + \boldsymbol{p}_i^- a_i)\cdot(\boldsymbol{p}_j^+ a_j^\dagger + \boldsymbol{p}_j^- a_j)\right]. \tag{2.31}$$

The quantum-mechanical equations of motion are

$$-i\frac{da_i^\dagger}{dt} = [H_2, a_i^\dagger],$$

$$-i\frac{da_i}{dt} = [H_2, a_i], \tag{2.32}$$

which can be written as

$$\frac{da_i}{dt} = i\left(\sum_j Q_{ij}a_j^\dagger + \sum_j P_{ij}a_j\right),$$

$$\frac{da_i^\dagger}{dt} = -i\left(\sum_j Q_{ij}^* a_j + \sum_j P_{ij}^* a_j^\dagger\right), \tag{2.33}$$

where $P_{ij} \equiv \lambda_i\delta_{ij} - J_{ij}(\boldsymbol{p}_i^+\cdot\boldsymbol{p}_j^-)$ and $Q_{ij} \equiv -J_{ij}(\boldsymbol{p}_i^+\cdot\boldsymbol{p}_j^+)$. We use a vector representation for the operators a_i and $a_i^\dagger$; that is, a and $a^\dagger$ are N-dimensional vectors whose components are a_i and $a_i^\dagger$, respectively. As N, the total number of (occupied) magnetic sites, is configuration dependent, so are all vectors and matrices in the following discussion. We write

$$\frac{d}{dt}\begin{pmatrix} a \\ a^\dagger \end{pmatrix} = i\begin{pmatrix} -P & -Q \\ Q^* & P^* \end{pmatrix}\begin{pmatrix} a \\ a^\dagger \end{pmatrix}, \tag{2.34}$$

where we refer to P and Q as the "interaction matrices" of order $N\times N$. We can also write

$$H_2 = S(a^\dagger a)\tilde{H}\begin{pmatrix} a \\ a^\dagger \end{pmatrix}, \tag{2.35}$$

where the Hamiltonian matrix $\tilde{H}$ is defined in the $2N\times 2N$ space to be

$$\tilde{H} = \begin{pmatrix} -P & -Q \\ Q^* & P^* \end{pmatrix}. \tag{2.36}$$

In order to diagonalize $\tilde{H}$, we perform a Bogoliubov transformation that introduces new boson operators d and $d^\dagger$, as follows:

$$a = g^* d + f d^\dagger,$$

$$a^\dagger = f^* d + g d^\dagger. \tag{2.37}$$

f and g are $N \times N$ matrices to be determined and which must satisfy the boson commutation rules

$$g^* f^T - f g^\dagger = 0,$$

$$g^* g^T - f f^\dagger = 1, \tag{2.38}$$

where f^T is the transpose matrix of f. We can also write these relationships in matrix representation:

$$\tilde{E}\tilde{I}\tilde{E}^\dagger = \tilde{I}, \tag{2.39}$$

where

$$\tilde{E} = \begin{pmatrix} g^* & f \\ f^* & g \end{pmatrix}, \quad \tilde{I} = \begin{pmatrix} -1 & 0 \\ 0 & 1 \end{pmatrix} \tag{2.40}$$

are of dimensions $2N \times 2N$.

The aim of the Bogoliubov transformation is to diagonalize Eq. (2.34). Consequently we require

$$\frac{d}{dt}\begin{pmatrix} d \\ d^\dagger \end{pmatrix} = i\begin{pmatrix} -\Omega & 0 \\ 0 & \Omega \end{pmatrix}\begin{pmatrix} d \\ d^\dagger \end{pmatrix}, \tag{2.41}$$

where Ω is a diagonal matrix of eigenfrequencies. Using Eqs. (2.34) and (2.40) one obtains

$$\begin{aligned} \frac{d}{dt}\begin{pmatrix} g^* & f \\ f^* & g \end{pmatrix}\begin{pmatrix} d \\ d^\dagger \end{pmatrix} &= i\begin{pmatrix} g^* & f \\ f^* & g \end{pmatrix}\begin{pmatrix} -\Omega & 0 \\ 0 & \Omega \end{pmatrix}\begin{pmatrix} d \\ d^\dagger \end{pmatrix} \\ &= i\begin{pmatrix} -P & -Q \\ Q^* & P^* \end{pmatrix}\begin{pmatrix} g^* & f \\ f^* & g \end{pmatrix}\begin{pmatrix} d \\ d^\dagger \end{pmatrix}. \end{aligned} \tag{2.42}$$

Hence, the equation we ultimately have to solve is

$$\tilde{E}D = \tilde{H}\tilde{E}, \tag{2.43}$$

where we have defined the matrix of eigenfrequencies:

$$D = \begin{pmatrix} -\Omega & 0 \\ 0 & \Omega \end{pmatrix}. \tag{2.44}$$

With this method, we can calculate the zero-point quantum spin fluctuations to order $1/S$, and hence the expectation value for the spin on occupied site i (Ref. 44):

$$\langle S_i^z \rangle = S - \langle a_i^\dagger a_i \rangle = S - \sum_\nu |f_{i\nu}|^2. \tag{2.45}$$

With the expectation value $\langle S_i^z \rangle$ now defined in terms of $|f_{i\nu}|^2$, one can calculate the staggered magnetization, defined in either Eq. (2.20) for the finite t/U Hubbard model or Eq. (2.21) for the $t/U \to 0$ Heisenberg model. Formally speaking, in a thermodynamically large system, spins that reside on finite-size clusters and which are not connected to the percolating cluster do not participate to the symmetry breaking nor do they contribute to the average bulk staggered magnetization. Hence, to capture this physics in the present problem, and to proceed numerically, we first identify for a given realization of disorder a percolating cluster of sites connected via nearest-neighbor hopping. For each spin on the percolating cluster, $\langle S_i^z \rangle$ is determined from Eq. (2.45), summed over, and normalized by N, the total number of sites for that realization of disorder (percolating and not), to give $\langle \hat{M}_s \rangle$ from Eq. (2.20) (henceforth denoted M). One then repeats the calculation for many dilution configurations for a given x, performing a disorder average and obtaining both the averaged staggered magnetization on the percolating cluster, $[M(x)]_{\text{perc}}$, or the *bulk* staggered magnetization $[M(x)]$, averaged over all magnetic sites in the sample. We stress that, while the staggered magnetization on the percolating cluster, $[M(x)]_{\text{perc}}$, is the most relevant quantity for the numerical study, it is the average staggered magnetization over all Cu magnetic sites in the system, percolating and not, $[M(x)]$, which is accessible to experiment, and which is displayed in Fig. 1.

In the presence of interactions beyond $J_1(i,j)$, the only change in the details of the above method occur in the matrix elements of P and Q. The form of these matrices, taking into account the second (J_2), third (J_3), and ring (J_c) exchange interactions, is discussed next.

2. Calculation of the P and Q matrices

a. J_1: First NN. In this case the quadratic Hamiltonian reads

$$H_2(J_1) = S \sum_{\langle i,j \rangle} J_1(i,j)(a_i^\dagger a_i + a_j^\dagger a_j - a_i a_j - a_i^\dagger a_j^\dagger). \tag{2.46}$$

The P and Q interaction matrices then have the following forms:

$$P = \begin{pmatrix} \lambda_1 & & & \\ & \ddots & & \\ & & \ddots & \\ & & & \lambda_{L^2} \end{pmatrix}, \quad Q = \begin{pmatrix} 0 & & & \\ & \ddots & -J_1 & \\ & -J_1 & \ddots & \\ & & & 0 \end{pmatrix}, \tag{2.47}$$

where λ_i is defined in Eq. (2.30), and Q is a symmetric matrix $Q_{ij} = -J_1(i,j)$.

b. J_2: Second NN. In this case, we have

$$H_2(J_2) = -S \sum_{\langle\langle i,j \rangle\rangle} J_2(i,j)(a_i^\dagger a_i + a_j^\dagger a_j - a_i^\dagger a_j - a_j^\dagger a_i), \tag{2.48}$$

which leads to the following additions to the P and Q matrices:

$$P^{(2)} = \begin{pmatrix} \lambda_1^{(2)} & & & \\ & \ddots & -J_2 & \\ & -J_2 & \ddots & \\ & & & \lambda_{L^2}^{(2)} \end{pmatrix},$$

$$Q^{(2)} = \begin{pmatrix} 0 & & & 0 \\ \vdots & \ddots & & \vdots \\ \vdots & & \ddots & \vdots \\ 0 & & & 0 \end{pmatrix}. \tag{2.49}$$

$\lambda_i^{(2)}$ is defined in a similar way as for λ_i:

$$\lambda_i^{(2)} \boldsymbol{n}_i^0 \equiv \sum_{\langle\langle j\rangle\rangle} J_2(i,j)\boldsymbol{n}_j^0, \tag{2.50}$$

where $\langle\langle j\rangle\rangle$ indicates a sum over the second neighbors of site i.

c. J_3: Third NN. In this case, we have

$$H_2(J_3) = -S \sum_{\langle\langle\langle i,j\rangle\rangle\rangle} J_3(i,j)(a_i^\dagger a_i + a_j^\dagger a_j - a_i^\dagger a_j - a_j^\dagger a_i). \tag{2.51}$$

Hence the expression for the P and Q matrices are modified by

$$P^{(3)} = \begin{pmatrix} \lambda_1^{(3)} & & & \\ & \ddots & -J_3 & \\ & -J_3 & \ddots & \\ & & & \lambda_{L^2}^{(3)} \end{pmatrix},$$

$$Q^{(3)} = \begin{pmatrix} 0 & & & 0 \\ \vdots & \ddots & & \vdots \\ \vdots & & \ddots & \vdots \\ 0 & & & 0 \end{pmatrix}, \tag{2.52}$$

with $\lambda_i^{(3)}$ defined by

$$\lambda_i^{(3)} \boldsymbol{n}_i^0 \equiv \sum_{\langle\langle\langle j\rangle\rangle\rangle} J_3(i,j)\boldsymbol{n}_j^0, \tag{2.53}$$

where $\langle\langle\langle j\rangle\rangle\rangle$ indicates the third neighbors of site i.

d. J_c: Ring exchange interaction. To first order in $1/S$, the four-spin terms appearing in the Hamiltonian are decoupled into bilinear products of $a_i^\dagger a_j$. That is, to order $1/S$, the net effect of the ring exchange is to simply renormalize the J_1 and J_2 interactions.[36,37,42] The contribution of the ring exchange terms to the quadratic Hamiltonian is thus

$$\begin{aligned} H_2(J_c) = -S^3 \sum_{\langle i,j,k,l\rangle} J_c(i,j,k,l)[&(a_i^\dagger a_i + a_j^\dagger a_j + a_k^\dagger a_k + a_l^\dagger a_l) \\ &+ (a_i^\dagger a_k + a_k^\dagger a_i + a_j^\dagger a_l + a_l^\dagger a_j) - (a_i^\dagger a_j + a_j^\dagger a_i + a_i^\dagger a_l \\ &+ a_l^\dagger a_i + a_j^\dagger a_k + a_k^\dagger a_j + a_k^\dagger a_l + a_l^\dagger a_k)], \end{aligned}$$

where $J_c(i,j,k,l) = \epsilon_i\epsilon_j\epsilon_k\epsilon_l J_c$. The elements of the Bogoliubov transformation matrices g and f are thus modified by the configuration-dependent $H_2(J_c)$-induced renormalization of the first- and second-neighbor exchanges. In zero dilution, J_1 and J_2 are renormalized to[36,37,42]

$$J_1^{\text{eff}} = J_1 - 2S^2 J_c = J_1 - \frac{J_c}{2},$$

$$J_2^{\text{eff}} = J_2 - S^2 J_c = J_2 - \frac{J_c}{4}. \tag{2.54}$$

III. ALGORITHMIC CONSIDERATIONS

In order to obtain the quantum magnetization corrections in the disordered lattice, we have to solve the eigenvalue problem described in Eq. (2.43). Results in the thermodynamic limit are estimated by doing a finite-size scaling analysis for different system sizes. For each value of size and dilution, we generate many realizations of disorder after which we perform successively the disorder average and the finite-size scaling to the thermodynamic limit. Our algorithm is organized as follows for each value of the system size and dilution:

(1) generation of the diluted lattice and computational identification of the percolating cluster.

(2) calculation of the P and Q matrices [Eq. (2.34)].

(3) diagonalization of the matrix using LAPACK routines.

For a system of linear size L and dilution concentration x, for each site, we generate a random number r between 0 and 1. The site is considered as removed if $r \geq (1-x)$. For each realization of disorder, for which the number of sites, $N(L^2,x)$, is different, we first construct the percolating cluster. To do this, the undiluted sites are labeled from 1 to N. Starting from site 1, with coordinates (α,β), we verify if the neighbors $(\alpha \pm 1,\beta)$ and $(\alpha,\beta \pm 1)$ are occupied. If yes the label of the site is changed to 1. Moving to one of these sites, the procedure is repeated. If the cluster 1 terminates, the next cluster takes the number of the first occupied site encountered. Once all sites have been visited, the procedure is repeated taking an arbitrary starting point. If neighboring sites are occupied the indices of the two sites take the lowest of the two values. The procedure is repeated until no further evolution occurs. For the biggest cluster we then check for the existence of percolating pathways along the x and y directions. If a percolating cluster exists, then the matrix $\tilde{H}$ [Eq. (2.36)] is constructed.

The diagonalization of $\tilde{H}$ is performed using a FORTRAN 77 LAPACK double precision set of routines:

(1) DGEHD2 computes Hessenberg reduction of the $\tilde{H}$ matrix.

(2) DORGHR and DHSEQR lead to the Shur factorization.

(3) DTREVC gives the eigenvectors of the $\tilde{H}$ matrix.

From the results of the LAPACK routines we first construct a matrix of eigenvectors E of $\tilde{H}$. We order the columns of E so that the first column is an eigenvector corresponding to the lowest eigenfrequency, and the last column is an eigenvector corresponding to the highest eigenfrequency of $\tilde{H}$.

The matrix E is thus defined up to the subspaces of degenerate eigenvectors and the matrix D in Eq. (2.44) is the diagonal matrix of its eigenfrequencies:

$$EDE^{-1} = \tilde{H}. \tag{3.1}$$

However, knowledge of D and E does not completely solve the problem. In order to establish the elements of the Bogoliubov transformation, we must construct from E the matrix $\tilde{E}$ that satisfies both relation (2.39), coming from the boson commutation relations, and eigenvalue equation (2.44). That is,

$$\tilde{E}\tilde{I}\tilde{E}^{\dagger} = \tilde{I} \text{ and } \tilde{E}D\tilde{E}^{-1} = \tilde{H}. \tag{3.2}$$

We find $\tilde{E}$ through the application of a transformation

$$\tilde{E} = Edb, \tag{3.3}$$

where db is a block-diagonal matrix. Using commutation relation (2.39), one finds

$$db\tilde{I}db^{\dagger} = (M)^{-1}, \tag{3.4}$$

with

$$M = E^{\dagger}\tilde{I}E. \tag{3.5}$$

M is a Hermitian matrix obtained from the LAPACK routines. It is block diagonal, with blocks M_i of size $p_i \times p_i$, corresponding to a subspace of degenerate eigenvalues of $\tilde{H}$, of dimension p_i. The transformation matrix db is therefore also block diagonal, with corresponding blocks A_i. If the matrix E_i represents the subspace of eigenvectors, of dimensions $2N \times p_i$, the transformation gives $\tilde{E}_i = E_i A_i$. To find A_i, we need to solve

$$\pm A_i A_i^{\dagger} = M_i^{-1}, \tag{3.6}$$

where the sign $\pm$ depends on which sector of the eigenvalue matrix D in Eq. (2.44) the subspace belongs. The blocks M_i are first inverted and then diagonalized,

$$M_i^{-1} = K_i D_i K_i^{-1}. \tag{3.7}$$

The matrix D_i contains either positive or negative eigenvalues, depending on the sign of the eigenvalue of the subspace of $\tilde{H}$. From this we find the diagonal matrix $\sqrt{\pm D_i}$, where the sign $\pm$ is chosen so that the square root is real. A_i is finally found from

$$A_i = K_i \sqrt{\pm D_i} K_i^{-1}. \tag{3.8}$$

In this block-diagonal procedure the subspace corresponding to the Goldstone modes is explicitly excluded. All other operations are then mathematically well defined[55] and the Bogoliubov transformation is completely determined. A further summary of the calculation procedure can be found in Appendix A.

IV. RESULTS

We have calculated the quantum fluctuations of the magnetic ground states for a diluted spin system for two situations:

(1) $t/U \to 0$, Heisenberg limit—The results are compared with those obtained by Mucciolo *et al.*,[45] who performed a spin-wave calculation similar to ours. The motivation here is to validate the two sets of results against each other and to quantify finite-size effects and statistical errors. In this Heisenberg limit, the additional terms in magnetization operator (2.16) leading to inequality (2.21) are zero. This calibration allows us to confirm that there is indeed a discrepancy between the results from $1/S$ calculations[45] and those from quantum Monte Carlo simulations[30] in the Heisenberg limit.

(2) $t/U = 1/8$—This t/U value is close to the one found for La_2CuO_4 by Coldea *et al.*[36] ($t/U \simeq 1/7.35$).[56] By using this value, we can begin an investigation of the effects of farther-neighbor and ring exchange interactions in the experimentally relevant situation of Cu substitution by Mg and Zn in $La_2Cu_{1-x}(Mg/Zn)_xO_4$.

A. $t/U = 0$: Diluted Heisenberg model

The presence of dilution introduces statistical fluctuations in the ground-state magnetization due both to configurational variations for fixed number of magnetic sites and to the variation in the number of magnetic sites from one configuration to another. To combat this, we perform an average over a number of disorder configurations, $\mathcal{N}_0$, which increases with the dilution. We chose $\mathcal{N}_0$ to be the integer closest to $5000x$, where x is the concentration of missing magnetic sites. Averaging over the disorder we define the average number of sites for a given concentration as

$$\bar{N} \equiv \frac{1}{\mathcal{N}_0} \sum N(L^2,x) = (1-x)L^2, \tag{4.1}$$

where $N(L^2,x)$ is the number of sites for a system of size L and concentration x for a specific disorder realization. System sizes were studied from $L^2 = 10 \times 10$ to $L^2 = 34 \times 34$. A detailed discussion of the various contributions to the statistical errors can be found in Appendix B.

The ground-state magnetization is estimated by extrapolating the finite-size results to the thermodynamic limit. In order to do this we proceed in two steps:

(1) First we determine the staggered magnetization for the sites on the percolating cluster for each realization of disorder, from which the staggered magnetization averaged over all magnetic sites for a specific realization of disorder is obtained. We then make a disorder average over many realizations, calculating both the disorder-averaged staggered magnetization on the percolating cluster, $[M(x,L)]_{\text{perc}}$, and the experimentally relevant disorder-averaged bulk staggered magnetization $[M(x,L)]$. The errors on these measures are estimated as explained in Appendix B.

(2) This process is repeated for different system sizes for a given x and the results are extrapolated to the thermodynamic limit by making a least-squares fit of the form[57]

$$[M(x,L)]_{\text{perc}} = [M(x)]_{\text{perc}} + \frac{a}{L} + \frac{b}{L^2}. \tag{4.2}$$

The same procedure is used for $[M(x,L)]$.

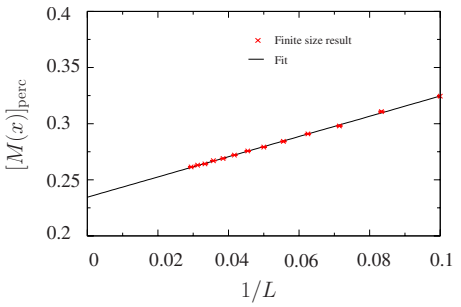

FIG. 5. (Color online) Staggered magnetization for the $t/U\rightarrow$ Heisenberg model for $x=20\%$ and $L\in[10,34]$.

As an example, we show results for $x=0.2$ in Fig. 5, where we plot the magnetization $[M(x,L)]_{\rm perc}$ against $1/L$. As one can see, the statistical noise on the data is small and is consistent with the size of the error bars estimated in Appendix B. The magnetization extrapolates linearly to the thermodynamic limit in $1/L$ to an excellent approximation, allowing a high-precision estimate for $[M]_{\rm perc}$:

$$[M(x=0.2)]_{\rm perc}=0.236\pm0.001. \tag{4.3}$$

We note that between $L=10$ and the biggest system size studied, $L=34$, $[M]_{\rm perc}$ varies by over 30%. This substantial variation confirms the need for such a finite-size scaling procedure here. Results for different values of x are shown in Fig. 6. For the system sizes studied, the size dependence is very nearly linear in $1/L$ for all x. One can also notice that the slope a is almost independent of x until the percolation threshold $x_p=0.41$ is approached, at which point it increases with finite-size effects becoming progressively more important. This evolution is not inconsistent with the critical nature of the percolation threshold, and the question as to whether $[M]_{\rm perc}$, determined via the $1/S$ method, goes continuously to zero or jumps discontinuously to zero at x_p is an intriguing one. On the other hand, it is found from quantum Monte Carlo simulations that $[M]_{\rm perc}$ has a discontinuous jump at $x=x_p$.[30] However, this question is not the main focus of the paper and to do it justice would require a more extensive and dedicated study near x_p. Here we simply remark that $[M]_{\rm perc}$

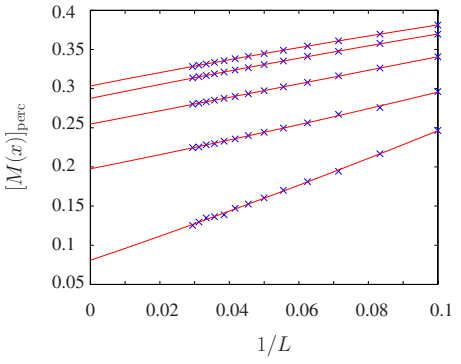

FIG. 6. (Color online) Evolution of $[M]_{\rm perc}$ for the $t/U\rightarrow$ Heisenberg model with L for different values of dilution—from top to bottom: $x=0\%$, $x=6\%$, $x=16\%$, $x=26\%$, and $x=36\%$.

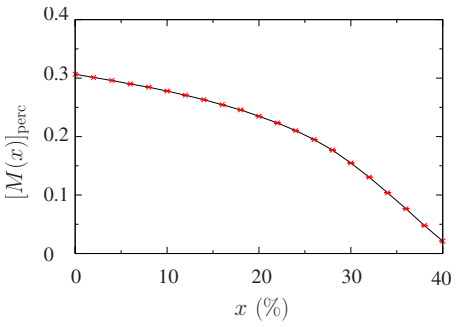

FIG. 7. (Color online) Staggered magnetization for the $t/U\rightarrow$ Heisenberg model on the percolating cluster extrapolated to the thermodynamic limit. The solid line is a guide for the eyes.

extrapolates to small values for concentrations less than, but near x_p.

Collecting all the results, we show the staggered magnetization for the ground state of the site-diluted Heisenberg model on the percolating cluster, $[M(x)]_{\rm perc}$, as a function of dilution in Fig. 7. $[M]_{\rm perc}$ goes smoothly from the known value for the undiluted case in the $1/S$ approximation,[58–60] $[M]_{\rm perc}\approx0.303$, to zero for x very close to the site-dilution percolation threshold, x_p.

In Fig. 8, we compare our results with those obtained by Mucciolo *et al.*[45] for the same model. The data are normalized by the value $[M]_{\rm perc}(x=0)\equiv M(0)$. There is extremely good quantitative agreement between our results and theirs, providing strong evidence that the two methods give correct results for the $1/S$ method considered.

It is important here to make a comparison between our results and those from quantum Monte Carlo (QMC), which is in principle exact, apart from numerical error. Such a comparison is made in Fig. 9, where we show unnormalized data for the magnetic moment on the percolation cluster from our calculation, compared with the QMC data of Ref. 30. For zero dilution, the methods give very similar results. This is expected as it is known that $1/S^2$ contributions to the quantum fluctuations in this case are identically zero,[59,61,62] meaning that the difference between spin wave and QMC comes, to leading order, from $1/S^3$ contributions, which one might

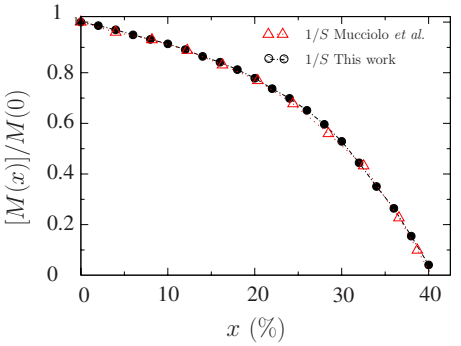

FIG. 8. (Color online) Comparison between our data for the ground-state (bulk-averaged) staggered magnetization for the Heisenberg model, normalized by the value at zero dilution, and the data of Mucciolo *et al.* (Ref. 45). The dashed-dotted line is a guide for the eyes.

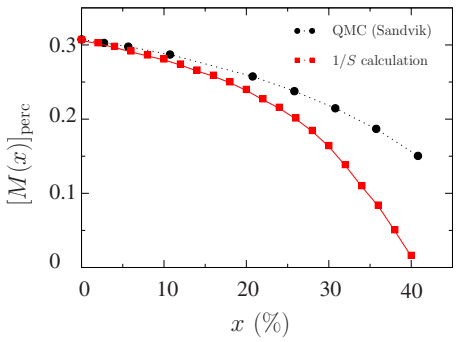

FIG. 9. (Color online) Staggered magnetization on the percolating cluster for the site-diluted Heisenberg model: comparison between QMC (from Ref. 30) and $1/S$ spin-wave results. The solid and dashed lines are guides for the eyes.

expect to be small. Moving away from zero dilution, the difference between the two sets of results increases in a monotonic way, with the moment from the QMC consistently larger than that determined from the $1/S$ spin-wave calculation. Hence the comparison explicitly illustrates that the $1/S$ method overestimates the importance of the quantum fluctuations in the presence of disorder. In order to understand this quantitative difference, one should investigate the effects of magnon-magnon interactions and Berry phase terms, which we do not attempt here.

The above limitations should be taken into consideration when comparing data from spin-wave calculations with the experiment. In Fig. 10 we add our results to those previously shown in Fig. 1 for comparison with the experimental neutron-scattering data on $La_2Cu_{1-x}(Mg/Zn)_xO_4$ (Ref. 31) and quantum Monte Carlo simulations.[30] The figure allows us to confirm the conclusion, already made in Ref. 45, that the extremely good agreement between experiment and the spin-wave calculation is rather fortuitous: if the Heisenberg Hamiltonian was an adequate starting point to describe the experimental data, the "exact" QMC results would be in better agreement with the experimental data than the $1/S$ spin-wave data are. As can be seen from the figure, the reverse is true; while the QMC data are consistently above the experimental curve, the spin wave-data lie very close to it. Hence, although the Heisenberg Hamiltonian is clearly a good starting point for acquiring an acceptable qualitative description of Mg- and Zn-doped La_2CuO_4 it appears, on the basis of the results shown in Fig. 10, to be inadequate for a really quantitative description. Further, we remark that the experimental data are presented such that they are normalized by $[M(x=0)]_{\mathrm{perc}}$. While the undiluted moment is $[M(x=0)]_{\mathrm{perc}} \approx 0.31$ from QMC and spin-wave calculations, recent estimates by Lee *et al.*[63] place the experimental moment at about 0.25. Hence, removing the absolute scale of the magnetic moment improves the impression of good agreement of the experiment with the QMC results for the site-diluted Heisenberg model for small x. When plotted on an absolute scale, the agreement between experiment and theory would be less convincing. This is an important point for the present paper as we continue to work within the linear spin-wave approximation and cannot expect to account for the contributions beyond $1/S$ linear spin waves which, as indicated by the QMC results, appear to be important for the dilution problem. That said, by making improvements to the starting spin-only description of the Hubbard Hamiltonian, through higher-order terms in the canonical transformation, we can expect to improve the comparison with experiment on an *absolute* $[M(x)]$ scale. With this in mind we have extended our calculations to order t^4/U^3, which allows us to include second- and third-neighbor exchanges as well as ring exchange around an elementary plaquette, and also to include quantum fluctuations from charge delocalization in the underlying Hubbard model.

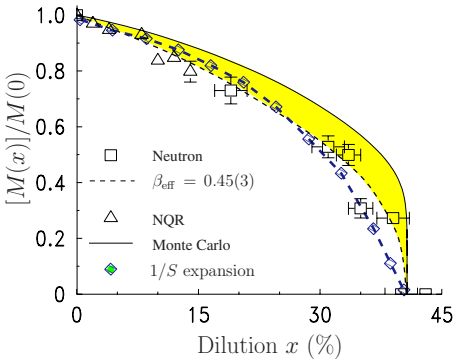

FIG. 10. (Color online) Ground-state magnetization as a function of dilution for Mg- and Zn-doped La_2CuO_4: $La_2Cu_{1-x}(Mg/Zn)_xO_4$ (Ref. 31), for quantum Monte Carlo (Ref. 30) for the site-diluted square lattice Heisenberg antiferromagnet (SLHAF). The dashed line is a guide for the eyes parametrized by $[M(x)]/M(0)=(1-x/x_p)^{\beta_{\mathrm{eff}}}$. The figure is reproduced from Ref. 31. Added to this figure is our data and that of Ref. 45 obtained from the numerical $1/S$ spin-wave analysis of the site-diluted SLHAF.

B. $t/U=1/8$: On the role of the ring exchange interaction

When interactions beyond nearest-neighbor exchange are taken into account, two effects have to be considered. First the transverse spin fluctuations are modified by the inclusion of the new interactions since these affect the magnon excitation spectrum.[36,47] Second, the charge delocalization induces a further quantum fluctuation term over and above those from transverse spin fluctuations. This is the difference between $\hat{M}_s$ and $\hat{\tilde{M}}_s$ in Eq. (2.20) and which leads to renormalization of the staggered magnetization in a way that depends on dilution. In this section, we treat these two effects separately to quantify their respective importance for $t/U=1/8$.

1. In the absence of charge mobility renormalization

a. Finite-size results. The first point we wish to illustrate here is the importance of the modification of the exchange pathways in the diluted system. We have argued in Sec. II C that dilution does not introduce *random* frustration at the classical level, even in the presence of farther-neighbor spin interactions, if these interactions are derived from the Hubbard model with nearest-neighbor hops only. In this case, such a longer-range interaction depends on the presence of a nearest-neighbor exchange pathway. Hence, we do not ex-

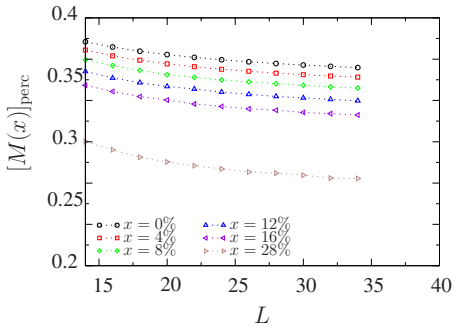

FIG. 11. (Color online) Size dependence of the staggered magnetization of the effective spin-only Hamiltonian $H_s^{(4)}$. Farther-neighbor interactions are generated through the existence of nearest-neighbor electronic hopping pathways. Charge-mobility-renormalization effects are not included here.

pect long-range interactions to have a destabilizing effect on classical Néel order on the percolating cluster. This can be seen indirectly by comparing the finite-size scaling of our effective spin-only model with that of a more phenomenological model. In the latter, which we refer to as the "p model," the farther-neighbor interactions have full strength, independently of the existence of a nearest-neighbor exchange path created by the electronic hopping processes, so that they exist even if the pathway is severed by a nonmagnetic defect (i.e., diluted site). In the p model, the bilinear exchange interactions J_2 and J_3 are taken to be $J_2 = 4t^4/U^3\epsilon_i\epsilon_j$ and $J_3 = 4t^2/U^3\epsilon_i\epsilon_k$, while J_c is kept to have the same site occupancy dependence as in Eq. (2.12). In Fig. 11, we show results for the size dependence of the staggered magnetization $[M]_{\rm perc}$ as a function of concentration x of diluted sites for the effective spin-only $H_s^{(4)}$ in Eq. (2.9) with $\{J_1, J_2, J_3, J_c\}$ coupling constants as given in Eqs. (2.9)–(2.12). The magnetization is a monotonic function of L for all values of x. This should be compared with Fig. 12, where we show similar data for the p model. For large dilution, the statistics are much worse and the magnetization considerably is lower than in Fig. 11. This indicates the buildup of random frustrated plaquettes that eventually destroy the Néel order *before* x_p is reached, even at the classical level.[21–26]

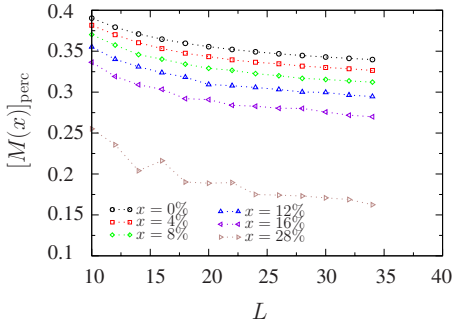

FIG. 12. (Color online) Size dependence of the staggered magnetization of a p-model Hamiltonian where farther-neighbor interactions are not explicitly dependent on the neighbor exchange hopping pathways.

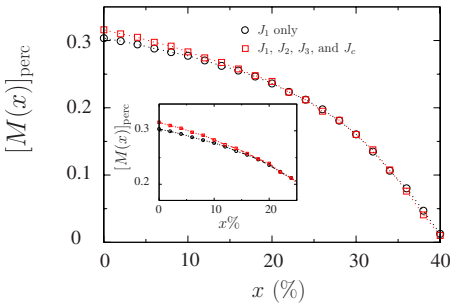

FIG. 13. (Color online) Dilution dependence of the staggered magnetization of the effective spin-only Hamiltonian obtained from the Hubbard model—no charge-renormalization effect. The inset shows a blowup for $x < 20\%$.

b. Thermodynamic limit. For the effective spin-only Hamiltonian, results are extrapolated to the thermodynamic limit, using the procedure described in Sec. IV B 1 a and Eq. (4.2). In Fig. 13 we show the ground-state magnetization $[M]_{\rm perc}$ compared with the previously shown results from Fig. 7 for the ($t/U \to$, J_1 only) Heisenberg model.

The first thing to notice is that there is very little difference with the Heisenberg model. The second is that the small difference that is present is toward a *higher* ground-state magnetization, with the maximum change occurring at $x = 0\%$. This is because the ring exchange terms decrease the transverse spin fluctuations.[42,47] As discussed in Refs. 42 and 47, this increase in the magnetic moment occurs because the ring exchange terms in $H_s^{(4)}$ decouple in the $1/S$ expansion into effective ferromagnetic second-neighbor two-body exchange terms which further stabilizes the two-sublattice Néel order by reducing the transverse spin fluctuations[42,47] [see Eq. (2.54)]. For x greater than about 12% dilution, this stabilization effect is largely destroyed and the two curves merge up to the percolation threshold. This is explained by the fact that, as these interactions involve more than two sites, they are more sensitive to dilution than the nearest-neighbor terms, and their effect becomes negligible long before the percolation threshold is reached. The effects at high dilution would be very different for the p model (see Fig. 12) with frustrating farther-neighbor interactions that are independent of the presence of nearest-neighbor exchange pathways. However, in the context of comparison with experimental results on $La_2Cu_{1-x}(Mg/Zn)_xO_4$, such terms should only appear through direct electronic hopping over farther neighbors in the Hubbard model. We have recently considered this problem in the absence of dilution,[47] but extending this work to include dilution is beyond the scope of the present study.

2. Finite charge mobility renormalization

The charge mobility, or electron delocalization effect, leads to a decrease in the magnetization[42,47] [see Eq. (2.20)]. However, the delocalization is also conditioned by the allowed nearest-neighbor electronic hopping pathways and is consequently also dilution dependent. We have found that the finite-size scaling of the magnetization, as described by Eq.

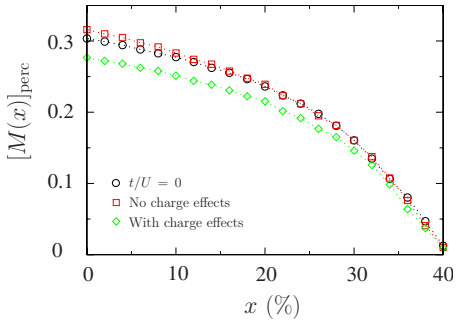

FIG. 14. (Color online) Evolution of the staggered magnetization with dilution for the effective spin-only Hamiltonian with charge mobility effects included. The open circles are the data for the Heisenberg ($t/U \to 0$) model (filled squares in Fig. 9 and open circles in Fig. 13). The diamonds and squares are the data for the spin-only representation of the $t/U=1/8$ site-diluted Hubbard model with and without (open squares in Fig. 13) finite charge mobility renormalization included, respectively.

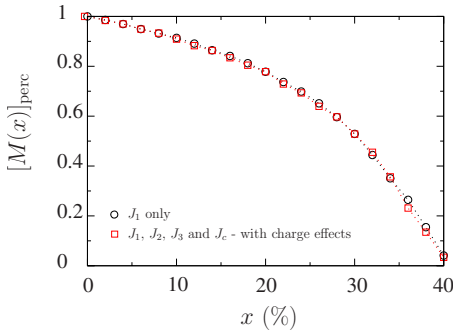

FIG. 15. (Color online) Data from Fig. 14 normalized by the ground-state order parameter at zero dilution, $M(x=0)$.

(4.2), is not changed qualitatively by this renormalization (not shown here) and the results are extrapolated to the thermodynamic limit using Eq. (4.2). As shown in Fig. 14, there is a significant decrease in the magnetization compared with $[M]_{\rm perc}$ without charge mobility renormalization, or with the Heisenberg model (see Fig. 13). This difference is again reduced as the dilution increases. For $x=0\%$ the decrease is on the order of 14%, whereas it goes down to 9.5% for $x=30\%$ and goes toward zero at the percolation threshold. We conclude therefore that the charge delocalization term is a major contribution to the corrections found by extending, to order t^4/U^3, the canonical transformation of the Hubbard model into an effective spin Hamiltonian. It is explicitly a property of the Hubbard model and is not present in a phenomenological spin-only model. It is therefore clear that care must be taken when using such phenomenological spin-only models without directly considering the mobility of the underlying system of electrons when aiming at obtaining a quantitative description and comparison between experiment and a microscopic theory. This is the main result of this paper.

C. Experimental considerations

Figure 14 illustrates our main result concerning comparison with experiment: inclusion of the charge-mobility-renormalization factor shifts the scale of magnetization downward over the whole dilution range. Comparing results for zero dilution, for the Heisenberg model, the ground-state moment is $[M_s] \approx 0.303$, while experiment yields $[M_s]_{\rm exp} \approx 0.25$.[63] Hence a comparison of $[M(x)]$ data not normalized by $M(x=0)$ will show the Heisenberg model, either from spin wave or from QMC, to be *above* those from the dilution experiments. Including hopping processes to order t^4/U^3 for $t/U=1/8$, a fair estimate for La_2CuO_4, one finds[36,47] $[M_s] \approx 0.27$. This is still above the experimental value, but it is clear that, taken altogether, the extra corrections arising from both transverse spin fluctuations and finite electron mobility away from the $t/U \to 0$ Heisenberg limit have scaled the magnetization in the right direction. This is an important result indicating that the canonical perturbation method proposed here can describe many of the magnetic features of $La_2Cu_{1-x}(Mg/Zn)_xO_4$.

We replot in Fig. 15 the data of Fig. 14 now normalized by the ground-state order parameter at zero dilution, $M(x=0)$. The two data sets for the Heisenberg (J_1 only) model and that for the spin model $H_s^{(4)}$ with farther-neighbor interactions, with the effects of electron delocalization via virtual hopping included, lie on top of each other. Hence, the improvements brought in by developing the effective spin description of the Hubbard model up to four virtual hopping terms, including ring exchange, are not evident when the data are normalized in this way. The data sets would therefore continue to give the same favorable but fortuitous comparison with the experimental data of Vajk *et al.*,[31] as seen in Fig. 10 and discussed in Ref. 45.

V. CONCLUSIONS AND PERSPECTIVES

A. Conclusions

In this paper we investigated the problem of site dilution in systems described by the half-filled one-band Hubbard model. We extended the canonical transformation technique to calculate an effective spin Hamiltonian up to order t^4/U^3, for magnetic site dilution x. We used a real-space spin-wave technique, linear in $(1/S)$ to calculate the dilution dependence of quantum fluctuations on the staggered magnetization. Specifically, we considered two problems. We first studied the Heisenberg $t/U \to 0$ limit, comparing our results with those from QMC studies[30] on the same model. We confirm, to a high degree of accuracy, previous results from Ref. 45, using a similar $1/S$ technique. Hence, our results also confirm a systematic deviation between the QMC (Ref. 30) and the spin-wave results for finite dilution. This difference, which is small for zero dilution, illustrates the dilution-dependent generation of magnon-magnon interactions and Berry phase terms, both of which are neglected in the $1/S$ spin-wave calculation. By comparing the QMC results and the $1/S$ results, one concludes that these two effects work to stabilize the semiclassical two-sublattice Néel order rather than to drive the system into an exotic quantum phase. Hence, while the spin-wave technique predicts the magnetic moment on the percolating cluster going to zero at, or very

close to, the percolation threshold, QMC simulations find a renormalized classical result, with the moment on the percolating cluster taking a discontinuous jump to zero at the percolation threshold.

The second and main objective of our work was to investigate how corrections to a site-diluted spin-only Hamiltonian, originating from a site-diluted one-band Hubbard model, affects the dilution dependence of the Néel order parameter (staggered magnetization $[M(x)]$). Underlying this question, was the goal of obtaining some information on the capacity of the one-band Hubbard model to describe data from experiments on site-diluted La_2CuO_4, $La_2Cu_{1-x}(Mg/Zn)_xO_4$.[31]

Within the one-band Hubbard model, the best estimates from fitting to magnon excitation spectra[36,47] give $t/U \approx 1/8$, placing the system away from the Heisenberg limit and into the intermediate-coupling regime, where higher-order electron correlations need to be taken into account. Integrating out the kinetic degrees of freedom via a canonical transformation, implemented to order t^4/U^3, introduces second- and third-neighbor interactions into the resulting spin-only Hamiltonian, as well as ring exchange term from electronic pathways around a closed square plaquette. Calculation of the magnetization operator for the original Hubbard model introduces at this order a charge mobility term that renormalizes the magnetization below that obtained by considering the (trivial) definition of the staggered magnetization of a spin-only Hamiltonian given by Eq. (2.21). Including all these effects, and staying within the linear $(1/S)$ spin-wave approximation, we find a reduced estimate for the moment at zero dilution, $\approx 0.27\mu_B$, compared with $0.31\mu_B$ for the Heisenberg model.[42] As farther-neighbor and ring exchange interactions mediated by four electronic hops require unbroken exchange pathways over length scales greater than nearest neighbor, their effects disappear well before the percolation threshold is reached. The net result is therefore that the evolution of the ground-state moment as a function of dilution is qualitatively similar to that for the Heisenberg model, disappearing at the percolation threshold in the same way, but with the absolute scale renormalized *downward* by 10%–15%. While the $1/S$ method is subject to the limitations described above, our results clearly illustrate that for an ultimate detailed and *quantitative* understanding of the role of site dilution in a correlated electron system, such as $La_2Cu_{1-x}(Mg/Zn)_xO_4$, the charge mobility effects must be taken into account. Such a description is beyond a spin-only model, decoupled from an electronic model describing the behavior of the strongly correlated electrons.

B. Perspectives

To expand on the work presented in this paper, it would be interesting to carry out further theoretical and numerical studies using a common calculation scheme for both the site-diluted Hubbard model expressed in the framework of a spin-only Hamiltonian with ring exchange and the site-diluted Heisenberg $(t/U \to 0)$ model. However, in the absence of a solution to the sign problem for frustrated quantum spin systems, quantitative results for the generalized dilution problem from large quantum Monte Carlo simulations will remain inaccessible for some time.

Angle-resolved photoemission spectroscopic (ARPES) experiments as well as *ab initio* calculations on a number of copper oxide materials provide strong evidence that an effective one-band Hubbard model description of these systems must include direct hopping parameters t' and t'' to second- and third-nearest-neighbor sites. Furthermore, such experiments and calculations indicate that these parameters are not significantly smaller than the nearest-neighbor hopping t, with $t'/t \sim -0.3$ and $t''/t \sim 0.15$. We have recently included direct hopping parameters t' and t'' in a derivation of a spin-only Hamiltonian representation of the half-filled t-t'-t''-U Hubbard model.[47] As a result of these sizable energy scales, our analysis of magnon excitation spectra in La_2CuO_4 reveals that the contributions from these parameters are of similar magnitude to the four hop (of order $1/U^4$) processes for nearest-neighbor hopping, which give rise to the ring exchange interactions studied in Ref. 36 and in the present paper [last term in $H_s^{(4)}$ of Eq. (2.9)].

A key result of Ref. 47 is that the ground-state staggered moment, approximately 0.235, is further reduced from the value found for the t-U Hubbard model, ~0.27, using the t and U values of Coldea *et al.*[36] This value is closer to but undershoots the experimental estimate of 0.25.[63] Although this progression lies within the experimental uncertainty, the detailed analysis of Ref. 47 suggests that the t-t'-t''-U Hubbard model is an improved starting point for a quantitative description of the magnetic properties of La_2CuO_4. This conclusion is in accordance with ARPES studies and *ab initio* calculations on various cuprates.

A natural extension of the work presented in this paper would be to investigate the role of t' and t'' in the site-dilution problem. In this model a large number of different ring exchange terms are generated[47] and the farther-neighbor hopping terms allow for connected pathways for dilution concentrations above the nearest-neighbor percolation threshold. It seems likely that these extra terms would change the shape of the $[M_s(x)]$ vs x curve, especially for x close to x_p, and hence change the qualitative aspect of the results even when the magnetization scale is factorized out of the problem, as in Fig. 15.

The realization that t' and t'' are important energy scales in a Hubbard model description of La_2CuO_4 leads to an interesting experimental puzzle when considering the substitution of Cu^{2+} by nonmagnetic Zn^{2+} and/or Mg^{2+}. As discussed earlier in this paper, and as illustrated by the convergence of the results of Fig. 13 for the Heisenberg model (J_1 only) and the $t/U=1/8$ Hubbard model (J_1, J_2, J_3, and J_c), the dilution dependence of the electronic hopping pathways leads to a crossover concentration x^* ($x^* \sim 15\%$ for $t/U=1/8$) above which the influence of the $J_2-J_3-J_c$ terms of order $1/U^3$ has essentially vanished. However, the presence of direct t' and t'' hoppings leads to additional *frustrating* second- and third-nearest neighbor exchanges with $J_2' \approx 4(t')^2/U$ and $J_3'' \approx 4(t'')^2/U$, respectively. Unlike the J_2 and J_3 interactions generated by fourth-order hopping processes, J_2' and J_3'' *do not depend* on the presence of nearest-neighbor pathways and hence are unaffected by the dilution (see discussion in Sec. IV B 1 and the one accompanying Fig. 12). As there is

now frustration which is independent of the existence of nearest-neighbor pathways, one would expect that upon dilution there would be a proliferation of Villain canted states[21–26] as the concentration of impurities approaches the percolation threshold x_p. This could ultimately lead to a Heisenberg spin-glass phase for a dilution concentration $x < x_p$. In this context, it is perhaps surprising that experiments find sharp (resolution-limited) magnetic Bragg peaks in $La_2Cu_{1-x}(Mg/Zn)_xO_4$ all the way to $x=x_p$.[31] It would certainly be interesting to revisit this question and study in more detail the possibility of a spin-glass phase developing in $La_2Cu_{1-x}(Mg/Zn)_xO_4$ close to the percolation threshold. We note further that in the region close to the percolation threshold there is the possibility of a freezing transition of the transverse spin components only. Such a transition could be observable in nuclear-quadrupolar-resonance (NQR) or muon-spin-relaxation (μSR) experiments[64] as were done sometime ago on $La_2Cu_{1-x}Zn_xO_4$.[20] However, in those early experiments,[20] it now seems likely that the then detected transverse spin freezing was driven by doped holes introduced by an imperfect control of the oxygen stoichiometry in $La_2Cu_{1-x}(Mg/Zn)_xO_4$.[31,32] It would be interesting to repeat such NQR and μSR experiments on $La_2Cu_{1-x}(Mg/Zn)_xO_4$ samples of the same quality as those used in neutron-scattering experiments of Ref. 31.

Another effect that could be relevant for $La_2Cu_{1-x}(Mg/Zn)_xO_4$ is the local distortion of the lattice due to the small difference in the ionic radii between Cu^{2+} and Mg^{2+} or Zn^{2+}.[65,66] This difference could lead to a local modification of the hopping parameter t in the neighborhood of a site where a Cu^{2+} ion is replaced by a nonmagnetic ion (see Fig. 2 of Ref. 65). Such disorder-induced variations in the hopping parameters could then contribute to explain the difference between the experimental data and QMC data in Fig. 1. The importance of local distortions could perhaps be provided by local probe experiments such as μSR, NMR, or NQR. This problem may also be considered as a precursor to the study of disorder-induced static magnetism in cuprate superconductors.[67] In this case the inclusion of mobile holes makes it much more complicated. But the study of the diamagnetic dilution problem in $La_2Cu_{1-x}(Mg/Zn)_xO_4$ maintained at half filling could provide a useful framework on which to build.

In conclusion, we have explored in this work the problem of the evolution of the magnetic order in a spin-only representation of a site-diluted one-band Hubbard expressed in terms of a spin-only Hamiltonian, taking into account up to four hop processes. For a finite ratio of hopping constant to on-site Coulomb energy, t/U, the resulting spin Hamiltonian differs from the simpler site-diluted $S=1/2$ Heisenberg model, containing effective exchange coupling beyond nearest neighbor as well as ring exchange interactions. The long-range exchange interactions, the ring exchange, and the renormalization of the nearest-neighbor exchange depend specifically on the local random hopping pathways that remain uninterrupted by the missing (diluted) sites. We hope that this study can motivate further analytical and numerical studies of the site-diluted one-band Hubbard model as well as new experiments on $La_2Cu_{1-x}(Mg/Zn)_xO_4$ in the vicinity of the percolation threshold.

ACKNOWLEDGMENTS

It is a pleasure to thank A.-M. S. Tremblay for a related collaboration leading to Refs. 42 and 47 as well as for useful comments on this paper. We also thank G. Albinet, B. Castaing, A. Castro Neto, F. Delduc, T. Devereaux, A. Mucciolo, L. Raymond, A. Sandvik, R. Scalettar, O. Vajk, and T. Vojta for useful discussions. Partial support for this work was provided by NSERC of Canada, the Canada Research Chair Program (Tier I) (M.J.P.G.), Research Corporation, the Province of Ontario (M.J.P.G.), and a Canada-France travel grant from the French Embassy in Canada (M.J.P.G. and P.C.W.H.). M.J.P.G. acknowledges the Canadian Institute for Advanced Research (CIFAR) for support.

APPENDIX A: CALCULATION PROCEDURE FOR THE BOGOLIUBOV TRANSFORMATION

We summarize below the steps required to obtain the eigenvector matrix for $\tilde{H}$, $\tilde{E}$, satisfying the boson commutation relations (2.38):

(1) Diagonalize $\tilde{H}$ using the LAPACK routines. This yields a set of eigenvalues ω_i with corresponding eigensubspaces generated by the eigenvectors E_i^n, where $n \in \{1, p_i\}$ and where p_i is the degeneracy of the eigenvalue and dimension of the subspace.

(2) For the subspace i define E_i, a $2N \times p_i$ matrix of the corresponding eigenvectors E_i^n. Form the block matrix M_i,

$$M_i = E_i^\dagger \tilde{I} E_i, \tag{A1}$$

of size $p_i \times p_i$.

(3) Invert M_i to get M_i^{-1}.

(4) Diagonalize M_i^{-1}, thus defining K_i and D_i:

$$M_i^{-1} = K_i D_i K_i^{-1}. \tag{A2}$$

(5) Define the matrix:

$$A_i = K_i \sqrt{\pm D_i} K_i^{-1}. \tag{A3}$$

(6) In this expression, the sign $\pm$ corresponds to the sign of ω_i.

(7) Define the new matrix of eigenvectors for the subspace i, $\tilde{E}_i$:

$$\tilde{E}_i = E_i A_i. \tag{A4}$$

(8) Repeat subspace by subspace to construct the eigenvector matrix $\tilde{E}$.

APPENDIX B: STATISTICAL ERRORS

In this section we discuss the origin of statistical errors in the numerics. Consider, as an example, the lattice of size $L^2=24\times 24$. For $x=12\%$, we studied $\mathcal{N}_0=620$ different realizations of disorder. The average magnetization and root-mean-square (rms) variation ΔM were found to be

$$[M(x=12\%, L=24)]_{\text{perc}} = 0.305, \quad \Delta M = 0.0052, \tag{B1}$$

from which we estimate the error on the measure to be $\pm\sigma_{M(x)}$,[68]

TABLE I. Staggered magnetizations for $L^2=24\times 24$ and $x \in [0,40]\%$.

x (%)	$[M]_{\mathrm{perc}}$	ΔM	$\frac{\Delta M}{[M]_{\mathrm{perc}}}$ (%)
0	0.338	0	0
2	0.334	0.0014	0.419
4	0.329	0.0022	0.668
6	0.324	0.0028	0.864
8	0.319	0.0036	1.128
10	0.313	0.0041	1.310
12	0.305	0.0052	1.705
14	0.298	0.0060	2.013
16	0.290	0.0070	2.414
18	0.281	0.0080	2.847
20	0.272	0.0096	3.529
22	0.261	0.0109	4.176
24	0.249	0.0135	5.421
26	0.236	0.0154	6.525
28	0.221	0.0183	8.281
30	0.204	0.0213	10.440
32	0.186	0.0237	12.742
34	0.166	0.0274	16.506
36	0.147	0.0291	19.795
38	0.125	0.0316	25.280
40	0.109	0.0330	30.275

$$\sigma_{M(x)} = \frac{\Delta M_s}{\sqrt{\mathcal{N}_0}}. \tag{B2}$$

In this example the estimated error is thus extremely small, around 0.1%, and the errors rise to around 1% near the percolation threshold. This small error estimate is consistent with the statistical fluctuations observed in Figs. 5 and 7.

For the example considered above, the ratio of the dispersion to the mean value is

$$\frac{\Delta M}{[M]_{\mathrm{perc}}} = 1.705\%. \tag{B3}$$

The ratios of the dispersion ΔM to mean value $[M]_{\mathrm{perc}}$ for fixed dilution L as a function of x and for fixed x as a function of L are shown in Tables I and II, respectively.

We can model this dispersion using three sources of variation: first, for a given x the number of magnetic sites varies from configuration to configuration. Second, for fixed N the number of sites on the percolating cluster will also vary. Third, there will also be a contribution from configurational fluctuations for a fixed number of sites. We stress that all these contributions are quantum in origin. That is, the classical ground state is perfectly ordered for all concentrations above the percolation threshold, as discussed in the main text. Hence at the classical level, changing the number of sites or local structures on the percolating cluster will not change the order parameter. However, the dilution reduces the local spin stiffness for spins in contact with nonmagnetic sites and increases the zero-point spin fluctuations. Hence these variations in number of sites and structure change the value of the order parameter. Indeed this point is already manifested by the fact that $[M]_{\mathrm{perc}}$ decreases with x.

TABLE II. Staggered magnetizations for $x=20\%$ and $L \in [10,34]$.

L	$[M]_{\mathrm{perc}}$	ΔM
10	0.325	0.0181
12	0.311	0.0166
14	0.298	0.0160
16	0.291	0.0134
18	0.284	0.0118
20	0.279	0.0114
22	0.276	0.0103
24	0.272	0.0096
26	0.269	0.0090
28	0.267	0.0079
30	0.264	0.0080
32	0.263	0.0075
34	0.261	0.0068

If $N_i(L^2,x)$ is the number of sites for realization i, and the mean number of sites is defined in Eq. (4.1), then for the example considered we find

$$\bar{N}(L=24,x=12\%) = 506.8 \pm 7.7. \tag{B4}$$

Hence

$$\frac{\Delta \bar{N}}{\bar{N}} = 1.51\%. \tag{B5}$$

To check the importance of fluctuations in the number of participating sites on the percolating cluster, $(N_{\mathrm{perc}})_i$, we analyze the ratio $\frac{(N_{\mathrm{perc}})_i}{N_i}$, where the subscript i labels a given realization of site dilution. We find

$$\frac{(N_{\mathrm{perc}})_i}{N_i} = 0.999 \pm 6.67 \times 10^{-3}. \tag{B6}$$

Equation (B6) was obtained after performing an average over the realizations of disorder (dilution) of $\frac{\mathrm{perc}_i}{N_i}$. This gives

$$\frac{\Delta \frac{N_{\mathrm{perc}}}{N}}{\frac{N_{\mathrm{perc}}}{N}} = 0.6\%. \tag{B7}$$

For a fixed number of magnetic sites, we can define the quantity

$$\left(\frac{\Delta M}{[M]_{\mathrm{perc}}}\right)_{\mathrm{mag}}$$

as a measure of the configurational contribution to the dispersion in ground-state order-parameter values, where

$(\cdots)_{\mathrm{mag}}$ is the disorder average over the restricted set of configurations with N_i=const. For the example discussed here we find

$$\left(\frac{\Delta M}{[M]_{\mathrm{perc}}}\right)_{\mathrm{mag}} = 0.4677\%, \tag{B8}$$

from which we estimate the total dispersion

$$\left(\frac{\Delta M}{[M]_{\mathrm{perc}}}\right)_{\mathrm{tot}} = \frac{\Delta \bar{N}}{\bar{N}} + \frac{\Delta \frac{N_{\mathrm{perc}}}{N}}{\frac{N_{\mathrm{perc}}}{N}} + \left(\frac{\Delta M}{[M]_{\mathrm{perc}}}\right)_{\mathrm{mag}} \simeq 2\%, \tag{B9}$$

in good agreement with Eq. (B3). The analysis can be generalized to the other values of x and L. For example, for $L^2 = 24 \times 24$ and $x=30\%$ we have

$$\frac{\Delta \bar{N}}{\bar{N}} = 3.48\%,$$

$$\frac{\Delta \frac{N_{\mathrm{perc}}}{N}}{\frac{N_{\mathrm{perc}}}{N}} = 1.41\%,$$

$$\left(\frac{\Delta M}{[M]_{\mathrm{perc}}}\right)_{\mathrm{mag}} = 5.45\%, \tag{B10}$$

which correspond to $\left(\frac{\Delta M}{[M]_{\mathrm{perc}}}\right)_{\mathrm{tot}} \simeq 10\%$, as obtained in Table I. Hence this analysis seems to account for the dispersion in magnetization values to a good level of approximation. The three sources of dispersion are of the same order of magnitude as long as one remains well away from the percolation threshold. At low defect concentration (small x), it is the fluctuations in the number of magnetic sites that dominate. As x increases the fluctuations increase, as one might expect as one approaches the critical percolating regime, and at large x it is the configurational contribution for fixed particle number which dominates. At 40% dilution the dispersion in values approaches 30% of the mean order-parameter value. Despite this large dispersion for this value of x, the number of configurations, $\mathcal{N}_0=2000$, is large enough to keep the estimated error at the 1% level.

[1] G. Grinstein, in *Fundamental Problems in Statistical Mechanics VI*, Proceedings of the Sixth International Summer School, Trondheim, Norway, 1984, edited by E. G. D. Cohen (North-Holland, Amsterdam, 1985).
[2] *Ill-Condensed Matter*, Ecole D'été de Physique Théoretique, Les Houches, 3 July–18 August 1978, edited by R. Balian, R. Maynard, and G. Toulouse (North-Holland, Amsterdam, 1979).
[3] A. Harris, J. Phys. C **7**, 1671 (1974).
[4] Y. Imry and S.-K. Ma, Phys. Rev. Lett. **35**, 1399 (1975).
[5] K. Binder and A. P. Young, Rev. Mod. Phys. **58**, 801 (1986).
[6] P. W. Anderson, Science **235**, 1196 (1987).
[7] S. Sachdev, Nat. Phys. **4**, 173 (2008).
[8] E. F. Shender and S. A. Kivelson, Phys. Rev. Lett. **66**, 2384 (1991).
[9] S. Eggert and I. Affleck, J. Magn. Magn. Mater. **272-276**, E647 (2004).
[10] J. Sirker, S. Fujimoto, N. Laflorencie, S. Eggert, and I. Affleck, J. Stat. Mech.: Theory Exp. (2008) P02015.
[11] M. Azuma, Y. Fujishiro, M. Takano, M. Nohara, and H. Takagi, Phys. Rev. B **55**, R8658 (1997).
[12] S. Wessel, B. Normand, M. Sigrist, and S. Haas, Phys. Rev. Lett. **86**, 1086 (2001).
[13] A. W. Sandvik and M. Vekic, Phys. Rev. Lett. **74**, 1226 (1995).
[14] R. Yu, T. Roscilde, and S. Haas, Phys. Rev. B **73**, 064406 (2006).
[15] S. Ghosh, T. F. Rosenbaum, G. Aeppli, and S. N. Coppersmith, Nature (London) **425**, 48 (2003).
[16] M. A. Metlitski and S. Sachdev, Phys. Rev. B **76**, 064423 (2007).
[17] A. Chakraborty, A. J. Epstein, M. Jarrell, and E. M. McCarron, Phys. Rev. B **40**, 5296 (1989).
[18] S. W. Cheong, A. S. Cooper, L. W. Rupp, B. Batlogg, J. D. Thompson, and Z. Fisk, Phys. Rev. B **44**, 9739 (1991).
[19] C. C. Wan, A. B. Harris, and J. Adler, J. Appl. Phys. **69**, 5191 (1991).
[20] M. Corti, A. Rigamonti, F. Tabak, P. Carretta, F. Licci, and L. L. Raffo, Phys. Rev. B **52**, 4226 (1995).
[21] J. Villain, Z. Phys. B **33**, 31 (1979).
[22] K. Binder, W. Kinzel, and D. Stauffer, Z. Phys. B **36**, 161 (1979).
[23] G. N. Parker and W. M. Saslow, Phys. Rev. B **38**, 11718 (1988).
[24] W. M. Saslow and G. N. Parker, Phys. Rev. B **38**, 11733 (1988).
[25] J. Vannimenus, S. Kirkpatrick, F. D. M. Haldane, and C. Jayaprakash, Phys. Rev. B **39**, 4634 (1989).
[26] P. Gawiec and D. R. Grempel, Phys. Rev. B **44**, 2613 (1991).
[27] Y.-C. Chen and A. H. Castro Neto, Phys. Rev. B **61**, R3772 (2000).
[28] A. L. Chernyshev, Y. C. Chen, and A. H. Castro Neto, Phys. Rev. B **65**, 104407 (2002).
[29] K. Kato, S. Todo, K. Harada, N. Kawashima, S. Miyashita, and H. Takayama, Phys. Rev. Lett. **84**, 4204 (2000).
[30] A. W. Sandvik, Phys. Rev. B **66**, 024418 (2002).
[31] O. P. Vajk, P. K. Mang, M. Greven, P. M. Gehring, and J. W. Lynn, Science **295**, 1691 (2002).
[32] O. P. Vajk, M. Greven, P. K. Mang, and J. W. Lynn, Solid State Commun. **126**, 93 (2003).
[33] S. Notbohm *et al.*, Phys. Rev. Lett. **98**, 027403 (2007).
[34] A. Gößling, U. Kuhlmann, C. Thomsen, A. Löffert, C. Gross, and W. Assmus, Phys. Rev. B **67**, 052403 (2003).
[35] M. Roger, J. Phys. Chem. Solids **66**, 1412 (2005).
[36] R. Coldea, S. M. Hayden, G. Aeppli, T. G. Perring, C. D. Frost, T. E. Mason, S.-W. Cheong, and Z. Fisk, Phys. Rev. Lett. **86**,

5377 (2001).
[37] A. M. Toader, J. P. Goff, M. Roger, N. Shannon, J. R. Stewart, and M. M. Enderle, Phys. Rev. Lett. **94**, 197202 (2005).
[38] L. Raymond, G. Albinet, and A.-M. S. Tremblay, Phys. Rev. Lett. **97**, 049701 (2006).
[39] A. M. Toader, J. P. Goff, M. Roger, N. Shannon, J. R. Stewart, and M. M. Enderle, Phys. Rev. Lett. **97**, 049702 (2006).
[40] A. H. MacDonald, S. M. Girvin, and D. Yoshioka, Phys. Rev. B **37**, 9753 (1988).
[41] A. L. Chernyshev, D. Galanakis, P. Phillips, A. V. Rozhkov, and A.-M. S. Tremblay, Phys. Rev. B **70**, 235111 (2004).
[42] J.-Y. P. Delannoy, M. J. P. Gingras, P. C. W. Holdsworth, and A.-M. S. Tremblay, Phys. Rev. B **72**, 115114 (2005).
[43] R. G. Melko and R. K. Kaul, Phys. Rev. Lett. **100**, 017203 (2008).
[44] L. R. Walker and R. E. Walstedt, Phys. Rev. B **22**, 3816 (1980).
[45] E. R. Mucciolo, A. H. Castro Neto, and C. Chamon, Phys. Rev. B **69**, 214424 (2004).
[46] E. V. Castro, N. M. R. Peres, K. S. D. Beach, and A. W. Sandvik, Phys. Rev. B **73**, 054422 (2006).
[47] J.-Y. P. Delannoy, M. J. P. Gingras, P. C. W. Holdsworth, and A.-M. S. Tremblay, arXiv:0808.3167, Phys. Rev. B (to be published).
[48] A. B. Harris and R. V. Lange, Phys. Rev. **157**, 295 (1967).
[49] A. H. MacDonald, S. M. Girvin, and D. Yoshioka, Phys. Rev. B **41**, 2565 (1990).
[50] A. H. MacDonald, S. Girvin, and D. Yoshioka, Phys. Rev. B **43**, 6209 (1991).
[51] P. Chandra and B. Doucot, Phys. Rev. B **38**, 9335 (1988).
[52] E. Dagotto and A. Moreo, Phys. Rev. Lett. **63**, 2148 (1989).
[53] A. P. Young, in *Strongly Interacting Fermions and High T_c Superconductivity, Les Houches, 1991*, edited by B. Douçot and J. Zinn-Justin (North-Holland, Amsterdam, 1995).
[54] A. Chubukov, E. Gagliano, and C. Balseiro, Phys. Rev. B **45**, 7889 (1992).
[55] J. Y. Delannoy, Ph.D. thesis, ENS-Lyon, 2005.
[56] A recent study (Ref. 47) that incorporates the effect of second-(t') and third-nearest-neighbor (t'') hoppings also found that a value of $t/U \sim 1/8$ allows for a spin-only Hamiltonian whose magnon excitations suitably describe the spin waves of La_2CuO_4 (Ref. 36).
[57] D. A. Huse, Phys. Rev. B **37**, 2380 (1988).
[58] P. W. Anderson, Phys. Rev. **86**, 694 (1952).
[59] R. B. Stinchcombe, J. Phys. C **4**, L79 (1971).
[60] E. Manousakis, Rev. Mod. Phys. **63**, 1 (1991).
[61] J.-I. Igarashi, Phys. Rev. B **46**, 10763 (1992).
[62] J.-I. Igarashi and T. Nagao, Phys. Rev. B **72**, 014403 (2005).
[63] Y. S. Lee, R. J. Birgeneau, M. A. Kastner, Y. Endoh, S. Wakimoto, K. Yamada, R. W. Erwin, S.-H. Lee, and G. Shirane, Phys. Rev. B **60**, 3643 (1999).
[64] I. Mirebeau *et al.*, Hyperfine Interact. **104**, 343 (1997).
[65] T. Edagawa, Y. Fukumoto, and A. Oguchi, J. Magn. Magn. Mater. **310**, e406 (2007).
[66] C.-W. Liu, S. Liu, Y.-J. Kao, A. L. Chernyshev, and A. W. Sandvik, Phys. Rev. Lett. **102**, 167201 (2009), have recently explored how local impurities such as Mg^{2+} and Zn^{2+} in La_2CuO_4 can lead to some local random frustration.
[67] B. M. Andersen, P. J. Hirschfeld, A. P. Kampf, and M. Schmid, Phys. Rev. Lett. **99**, 147002 (2007).
[68] M. Boas, *Mathematical Methods in the Physical Sciences* (Wiley, New York, 1983).